Universidade de
Aveiro
Ano 2022

SOFIA PEREIRA VIEGAS

DESENVOLVIMENTO DE NOVOS MATERIAIS HÍBRIDOS CAPAZES DE INCORPORAR COMPOSTOS COM ATIVIDADE FARMACOLÓGICA

DEVELOPMENT OF NEW HYBRID MATERIALS CAPABLE OF INCORPORATING COMPOUNDS WITH PHARMACOLOGICAL ACTIVITY

Universidade de Aveiro
Ano 2022

SOFIA PEREIRA VIEGAS

DESENVOLVIMENTO DE NOVOS MATERIAIS HÍBRIDOS CAPAZES DE INCORPORAR COMPOSTOS COM ATIVIDADE FARMACOLÓGICA

DEVELOPMENT OF NEW HYBRID MATERIALS CAPABLE OF INCORPORATING COMPOUNDS WITH PHARMACOLOGICAL ACTIVITY

Dissertação apresentada à Universidade de Aveiro para cumprimento dos requisitos necessários à obtenção do grau de Mestre em Biotecnologia (ramo Industrial e Ambiental), realizado sob a orientação científica da Doutora Bárbara Joana Martins Leite Ferreira, Investigadora do Departamento de Química da Universidade de Aveiro/CICECO e do Doutor José Carlos Martins de Almeida, Investigador do Departamento de Engenharia de Materiais e Cerâmica da Universidade de Aveiro/CICECO.

Do the best you can until you know better. Then, when you know better, do better.

Maya Angelou

o júri

presidente

Doutor Manuel António Coimbra Rodrigues da Silva
Professor Associado com Agregação/ Departamento de Química da Universidade de Aveiro

vogais

Professora Doutora Maria Helena Figueira Vaz Fernandes
Professora associada do CICECO/Departamento de Materiais e Cerâmica da Universidade de Aveiro

Doutora Bárbara Joana Martins Leite Ferreira
Investigadora do CICECO/Departamento de Química da Universidade de Aveiro

agradecimentos

Antes de mais, quero deixar um especial agradecimento aos meus orientadores, por todo o apoio, paciência, dedicação e confiança que depositaram em mim. Doutora Bárbara Ferreira, por ser incansável no seu apoio e me motivar sempre a chegar mais longe. Doutor José Almeida, pela atenção, pela constante partilha de conhecimento e pela confiança em mim para desenvolver este projeto mesmo sendo fora da minha área de estudos. Ambos marcaram o meu percurso académico da melhor forma possível, e por isso o meu mais sincero obrigado.

Um profundo obrigado à Doutora Verónica Bastos e à Doutora Helena Oliveira, investigadoras do Departamento de Biologia (CESAM), por toda a simpatia, acompanhamento e apoio indispensável na realização dos ensaios celulares.
Ao Doutor Ricardo Vieira, por toda a prestabilidade e ajuda na análise matemática dos dados do trabalho. Ao meu colega de laboratório, Diogo Marinheiro, por estar sempre disponível para me ajudar e esclarecer. E a todos os técnicos que realizaram as análises descritas no trabalho ou que, de alguma forma, me ajudaram em todos os processos laboratoriais.

Um enorme agradecimento aos meus amigos, que sempre me incentivaram nos bons e maus momentos e se tornaram os meus melhores parceiros nesta aventura. À Ana Pinto, Ana Pereira, Inês, Colónia, Costa, Samuel e Sérgio, por me terem acompanhado durante toda esta etapa, sem vocês teria sido tudo muito menos divertido. Ao Renato, por ser o meu melhor amigo mesmo depois de o ter rejeitado no 10ºano. Ao Carlos Daniel por todos os factos sobre coelhinhos e peixes e coisas de biólogo. Ao Tomás e Afonso, pelas caminhadas que sempre me ajudaram a desanuviar e deixar os pensamentos negativos.

Agradeço do fundo do coração a toda a minha família, especialmente aos meus pais, por terem feito os maiores esforços possíveis para me permitirem seguir os meus sonhos e me inspirarem sempre a dar o melhor de mim. E, á minha irmã, e melhor amiga, por todos os momentos juntas e apoio incondicional.

Por fim deixo um agradecimento a todos os que não foram mencionados, mas que contribuíram direta ou indiretamente para a concretização deste trabalho.

palavras-chave

tecido ósseo, materiais híbridos, método sol-gel, sistema PDMS-SiO2, resveratrol, sistema de entrega de fármacos.

resumo

Apesar da sua capacidade intrínseca de regeneração após uma lesão, o tecido ósseo pode ser desafiado por uma enorme variedade de condições patológicas que levam a grandes perdas e impedem a sua regeneração, sendo necessária a aplicação de um substituto (implante) ósseo. Os recentes avanços no desenvolvimento de biomateriais, especificamente na área dos materiais híbridos, têm providenciado melhores alternativas aos implantes utilizados normalmente, oferendo amplas aplicações médicas na restauração do osso danificado. Neste trabalho focamo-nos especificamente num material híbrido composto por polidimetilsiloxano e tetraetilortosilicato. Este sistema, obtido através do método de sol-gel, permite a incorporação da componente orgânica numa rede inorgânica, com interações que levam à obtenção de materiais híbridos com morfologia e propriedades multifuncionais adequadas para aplicação óssea.

O resveratrol (RES) é uma molécula bioativa com múltiplas propriedades benéficas para a saúde humana, em específico, no metabolismo envolvido na regeneração óssea, tornando-o um excelente candidato para aplicação em terapias associadas a doenças ósseas. No entanto, as suas caraterísticas físico-químicas, especificamente a baixa solubilidade e biodisponibilidade, criam limitações à sua aplicação. Para combater estes problemas têm sido desenvolvidos sistemas de entrega de fármacos capazes de aumentar a absorção e ultrapassar as suas limitações.

Neste trabalho foi desenvolvido e caraterizado um novo material híbrido combinado com RES, com o objetivo de avaliar a capacidade do sistema para incorporar e libertar este composto. O RES foi carregado com elevada eficácia (eficácia de carregamento > 75%) nos materiais híbridos através da técnica do evaporador rotativo. A incorporação promoveu a sua amorfização e aumentou a solubilidade e libertação *in vitro* quando comparado com o RES livre (não encapsulado). Todos os perfis de libertação obtidos apresentaram uma dependência do pH e mostraram ser claramente mais rápidos em pH 5,2 do que em pH 7,4. A libertação de RES do material carregado foi gradual ao longo do tempo, apresentou um atraso inicial de aproximadamente 4 horas e foi bem descrita pelo modelo matemático de Weibull. Foram realizados estudos de citotoxicidade *in vitro* em células humanas de osteossarcoma (MG-63) e, estes mostraram uma diminuição da viabilidade celular com o aumento da concentração das amostras carregadas com RES (para concentrações > 100 $\mu g\ mL^{-1}$). Os materiais híbridos sem a adição de RES não apresentaram citotoxicidade independentemente da concentração estudada.

keywords

bone tissue, hybrid materials, sol-gel method, PDMS-SiO_2 system, resveratrol, drug delivery system.

abstract

Despite its intrinsic ability to regenerate after an injury, bone tissue can be challenged by a huge variety of pathological conditions that lead to massive bone loss, necessitating the application of a bone implant. Recent advances in the development of biomaterials, specifically in the area of hybrid materials, have provided better alternatives to commonly used implants, offering wide medical applications in the restoration of damaged bone. In this work we specifically focus on a hybrid material composed of polydimethylsiloxane and tetraethyl orthosilicate This system, obtained through the sol-gel method, allows the incorporation of the organic component in an inorganic network, with interactions that lead to the obtention of hybrid materials with morphology and multifunctional properties suitable for bone applications.

Resveratrol (RES) is a bioactive molecule with many beneficial properties for human health, specifically, in the metabolism involved in bone regeneration, making it an excellent candidate for application in therapies associated with bone diseases. However, its physicochemical characteristics, specifically the low solubility and bioavailability, create limitations to its application. To combat these problems, drug delivery systems capable of increasing absorption and overcoming the limitations of RES have been developed.

In this work, a new hybrid material combined with RES was developed and characterized, in order to evaluate the system's ability to incorporate and release this compound. RES was loaded with high efficiency (loading efficiency > 75%) into hybrid materials using the rotary evaporator technique. The incorporation promoted its amorphization and increased solubility and in vitro release when compared to free RES (non-encapsulated). All the release profiles obtained showed a pH dependence and were clearly faster at pH 5.2 than at pH 7.4. The release of RES from the loaded material was gradual over time, had an initial time lag of approximately 4 hours, and was well described by the Weibull mathematical model. In vitro cytotoxicity studies were performed on human osteosarcoma cells (MG-63) and these showed a decrease in cell viability with increasing concentration of RES-loaded samples (for concentrations > 100µg mL^{-1}). Hybrid materials without the addition of RES did not show cytotoxicity regardless of the concentration studied.

Table of contents

List of Figures III
List of Tables IV
List of Abbreviations V
I. Introduction 1
1. Background 1
2. Main objectives 2
3. Structure of the thesis 3
II. State of the Art 4
1. Bone tissue 4
2. Biomaterials for bone tissue engineering 5
2.1. Hybrid materials 7
2.2. Sol-gel method 8
2.3. Organically modified silicates (ORMOSILs) 10
2.3.1. PDMS- SiO_2 system 11
3 Resveratrol 14
3.1 Resveratrol in bone therapies 15
3.2 Resveratrol drug delivery systems 17
III. Experimental Procedure 19
1. Applied chemicals 19
2. Samples preparation 19
3. RES-loaded samples preparation 21
4. Physicochemical characterization 22
4.1. X-Ray Diffraction (XRD) analysis 22
4.2. Fourier Transform Infrared (FT-IR) spectroscopy 23
4.3. Specific Surface Area by the Brunauer-Emmett-Teller (BET) method 23
4.4. Scanning Electron Microscopy (SEM) 26
4.5. Thermogravimetric Analysis (TGA) 27
5. *In vitro* solubility and release assays 27
5.1. Solubility studies 27
5.2. *In vitro* release studies 27
6. Cell studies 28

6.1. Reagents 28
6.2. Cell culture and preparation of the samples 29
6.3. *In vitro* cell viability assay 29
IV. Results and Discussion 31
1. Characterization of PDMS-SiO_2 samples 31
1.1. XRD analysis 31
1.2. FT-IR spectroscopy analysis 32
1.3. BET analysis 34
2. Characterization of RES loaded samples 36
2.1 Loading efficiency and capacity 39
2. *In vitro* release studies 41
3.1. Solubility studies 41
3.2. *In vitro* RES release studies 42
4. Cell viability studies 47
V. Conclusions and future perspectives 49
References 51
Supplementary material i
Calibration curves for RES i
RES release studies spectra ii

List of Figures

Figure 1. Schematic overview of the bone tissue with its macroscopical composition. Adapted from [203]. 5
Figure 2. Schematic overview of the ideal synthetic bone graft properties. 7
Figure 3. Scheme of the classification of hybrid materials with an example of morphological structures of Class I and II hybrid materials. Adapted from [58] 8
Figure 4. Scheme of steps involved in the preparation of materials by the sol-gel process. Adapted from [50]....9
Figure 5. Scheme of a silica/polymer class II ORMOSIL [17]. 10
Figure 6. Hybrid structure of the PDMS-SiO_2 system with the organic (PDMS)-inorganic (SiO_2) bond. Adapted from[204]....12
Figure 7. Chemical structure of cis-(left) and trans-(right) RES [86]. 15
Figure 8. Experimental protocol used to prepare the PDMS-SiO_2 samples. 20
Figure 9. PDMS-SiO2 samples after being dried: (a) M0C0-I; (b) M0C0-II; (c) M0C0-III; (d) M0C0-IV. 21
Figure 10. Types of gas absorption isotherms, according to IUPAC's classification. 24
Figure 11. Different types of hysteresis, according to IUPAC's classification 26
Figure 12. XRD spectra of the PDMS-SiO_2 samples. 31
Figure 13. FT-IR spectra of the PDMS-SiO_2 samples in the intervals of: (a) 1500-4000 cm^{-1} (b) 300-1500 cm^{-1}. 34
Figure 14. Isotherms of the PDMS-SiO_2 samples obtained by the BET method. 35
Figure 15. XRD spectra of the PDMS-SiO_2-RES samples and T-RES. 36
Figure 16. FT-IR spectra of the samples in the interval of 300-4000 cm^{-1}. **(a)** M0C0-I, M0C0-I-RES, and T-RES **(b)** M0C0-III, M0C0-III-RES, and T-RES **(c)** M0C0-IV, M0C0-IV-RES, and T-RES. 38
Figure 17. SEM micrographs of the unloaded and loaded samples: (A1) M0C0-I; (A2) M0C0-I-RES; (B1) M0C0-III; (B2) M0C0-III-RES; (C1) M0C0-IV; (C2) M0C0-IV-RES. 39
Figure 18. TGA analysis of unloaded and loaded PDMS-SiO_2 samples and pure RES. 40
Figure 19. Solubility profiles of the RES loaded samples and pure RES at pH 7.4 after 24 hours. 41
Figure 20. Cumulative release of RES from the non-encapsulated (free RES) and encapsulated sample (M0C0-IV-RES) at pH 5.2 and 7.4. **(a)** Full 48 hours profile; **(b)** First 24 hours profile. 43
Figure 21. Fitting of each model (KP, NWF and Weibull) for sample M0C0-IV-RES and free RES at pH 5.2 and 7.4. 46
Figure 22. Effect of pristine M0C0-IV (0-400 µg/mL; **(a)**) , RES-loaded M0C0-IV (0–350 µg/mL, **(b)**), and bulk RES (0–500 µM, **(c)**) on cell viability of MG-63 osteosarcoma cells after 24h of exposure....48

Figure sm1. Calibration curve for RES at PBS pH 5.2. i
Figure sm2. Calibration curve for RES at PBS pH 7.4. i

Figure sm3. RES spectra obtained at various times for the sample M0CO-IV-RES at pH 5.2 (with the respective dilutions used)..... ii
Figure sm4. RES spectra obtained at various times for the sample M0CO-IV-RES at pH 7.4 (with the respective dilutions used)..... ii

List of Tables

Table 1. Composition of the PDMS-SiO_2 samples.....19
Table 2. Values of the maximum angle and distance between inorganic centres of the PDMS-SiO_2 samples.....32
Table 3. Values of surface area calculated from the nitrogen adsorption isotherms, for the PDMS-SiO_2 samples.....35
Table 4. Values of loading capacity and efficiency for the RES PDMS-SiO_2 loaded samples.....41
Table 5. Kinetic parameters and goodness of the fits of RES release from sample M0C0-IV-RES and pure RES.....47

List of Abbreviations

BET	Brunauer-Emmett-Teller
BCP	Bone cancer pain
BJH	Barrett, Joyner and Halenda
BMD	Bone mineral density
DDS	Drug delivery system
FT	Fourier transformation
FT-IR	Fourier transform infrared
HA	Hydroxyapatite
IPA	Isopropyl alcohol
IR	Infrared
IUPAC	International union of pure and applied chemistry
JCPDS	Joint committee on powder diffraction standards
MSNs	Mesoporous silica nanoparticles
ORMOSILs	Organically modified silicates
PBS	Phosphate buffered saline
PDMS	Polydimethylsiloxane
PMMA	Polymethyl methacrylate
RES	Resveratrol

SEM	Scanning electron microscopy
SSA	Specific surface area
TEOS	Tetraethyl orthosilicate
TGA	Thermogravimetric analysis
T-RES	*Trans*-resveratrol
XRD	X-ray diffraction

I. Introduction

1. Background

The increase in human longevity and the great scientific advances observed in recent years have led to a continuous search for new materials capable of offering a better quality of life. However, with the average life expectancy increasing more and more, it is highly expected that a large part of the world population will suffer from diseases that affect the skeleton (bones), with these pathologies being considered one of the main causes of disability [1]. Bone tissue damage or disorders/defects can have a wide variety of causes, from the acute ones such as fractures, to the chronic ones, i.e., osteoporosis [2], osteoarthritis [3] or cancers such as osteosarcoma [4].

Osteoporosis is a disease characterized by reduced bone mass and altered bone architecture, which subsequently leads to an increase in bone fragility and a higher risk of fractures. In 2019, it affected approximately 32 million individuals aged above 50 in Europe (plus Switzerland and United Kingdom), with related costs estimated to raise up to 1.4 billion euros in 2025 in Portugal only [5,6]. Osteosarcoma is a bone primary tumor that occurs most often between the ages of 10 and 19. Despite being a rare type of cancer, its mortality rate is still quite high, with a five-year survival rate (for patients diagnosed between 2000-2007) of only 54% in central Europe, further increasing the need for more effective options of treatment [7]. These disorders can lead to a subsequent bone loss and greatly impact the quality of life or even the economy, with high health care costs [8].

Despite the known bone self-healing (regeneration) capability this phenomenon is only observed when the length of the damage does not go beyond double the diameter of the affected bone. More significant defects can result in scar tissue formation or even in longstanding weaknesses, requiring clinical intervention, which results in a substantial burden for the patients. Several approaches using bone autografts, allografts, or synthetic bone substitutes are currently used to treat such significant defects [9,10]. Although these approaches have already been quite successful in saving and improving several lives through the years, their major limitations (such as high costs, risks of transplantation or the durability

of materials) make them insufficient solutions for the current needs [11]. These limitations led to the need to find new paths, in which biomaterials not only fulfil their functions at a structural level, by replacing the damaged tissue, as well as present a more functional role, focused on tissue regeneration [12,13], increasing the interest on materials capable of mimicking mechanical properties of bone tissue. In this context, a new family of hybrid materials, named organically modified silicates (ORMOSILs) came to light driven by the idea of sharing synergies between inorganic silica (SiO_4) domains and organic polymer domains.

In this work, we will be focusing on the PDMS-SiO2 system since it allows a combination of the mechanical and bioactive properties of its inorganic component (tetraethyl orthosilicate, TEOS), with the flexibility and controlled degradation rate of the organic part (polydimethylsiloxane, PDMS) [14]. The preparation of the organic-inorganic hybrid materials will be achieved by the sol-gel processing method that includes the hydrolysis and condensation reactions of metal alkoxides, in which the intervention of precursors or different synthesis conditions allows the formation of different types of materials with different characteristics and biological properties [15,16].

Resveratrol (RES), a stilbene polyphenol with higher clinical potential for bone tissue regeneration - and which has attracted increasing interest from the scientific community[19,20] - will be combined with the hybrid materials.

2. Main objectives

In this work, the PDMS-SiO_2 system was explored, using the specific properties of its organic and inorganic components in order to create a network with interactions between the components resulting in a material with tunable morphology, size, and multifunctional properties. The incorporation of RES into the ORMOSILs, and the physical, chemical, thermal and mechanical properties of the materials was evaluated. In vitro studies were also performed to assess the capacity of the system to load and release RES. This novel approach, which was never reported in literature, combines the physicochemical properties of the PDMS-SiO_2 system with the biological properties of RES, and could give rise to a bioactive hybrid material with ideal properties to be used as a synthetic bone graft and a drug delivery system (DDS) for RES.

To achieve this goal, the first step is to synthetize the materials, as described in section III. Experimental procedure, followed by a thorough characterization of the obtained materials using various methodologies - X-Ray Diffraction (XRD), Fourier Transform Infrared (FTIR) spectroscopy, specific surface area by the Brumauer-Emmet-Teller (BET), Scanning Electron Microscopy (SEM) and Thermogravimetric Analysis (TGA).

The loading of the synthetized materials with RES was performed using the rotary evaporation technique, followed by the characterization of the loaded materials and the determination of the loading capacity of each one. The release kinetics of the loaded materials was tested in two different pH values, 7.4, similar to the physiological pH, and 5.2, mimicking the acidic environment of some tumorous tissues. The cytotoxicity was tested on MG-63 cells to study the biocompatibility of the hybrid materials.

3. Structure of the thesis

The present thesis is divided into five main chapters. Chapter one, the present one, encompasses the background and the main objectives of this work. Chapter two presents a review of literature on bone tissue and related main problems, biomaterials (specifically hybrid materials) and the biological characteristics of resveratrol, as well as its advantages in terms of bone tissue applications. Chapter three focuses on the experimental procedure, where all the methods used to prepare and characterize the samples are explained. Chapter four presents the treatment of the results obtained and the respective discussion. And, lastly, chapter five describes the main conclusions and future perspectives of the work

II. State of the Art

1. Bone tissue

The human skeleton is responsible for approximately 15% of the total body weight and is considered an important structural tissue of the human body[17]. Its more conventional functions are the support and movement of the body, the protection of internal organs from possible external damage or the production and protection of the bone marrow[8,18]. However, the relevance of this organ goes far beyond this, and more recent studies demonstrate its importance for body homeostasis and for the maintenance of other vital organs/systems, such as the immune system, brain function or energy metabolism[18,19].

Bone is a mineralized tissue and, macroscopically, is composed by two structures: the cortical (compact) bone and the cancellous (spongy) bone, both mainly differentiated by their porosity and density (Figure 1). Cortical bone is located in the outer layer and is characterized by being dense, solid, and well vascularized and mineralized. Cancellous bone is constituted by an irregular and interconnected sponge-like structure and is located at the inner section. On the one hand, the cortical bone is denser and less flexible, on the other hand, the cancellous bone shows greater fragility, but its surface area contributes to the diffusion of nutrients and growth factors, thus demonstrating its greater metabolic activity[20,21].

Considering its constitution, bone tissue is composed of inorganic constituents (70%), organic constituents (20%) and water (10%). The mineral or inorganic phase is composed essentially by calcium phosphate (primarily, hydroxyapatite (HA), $Ca_{10}(PO_4)_6(OH)_2$) [22], and the organic phase is composed by proteins (mainly type I collagen fibbers). This conjunction between inorganic and organic components give rise to the physical and chemical characteristics of bone tissue that are essential to its proper functioning and performance[23,24].

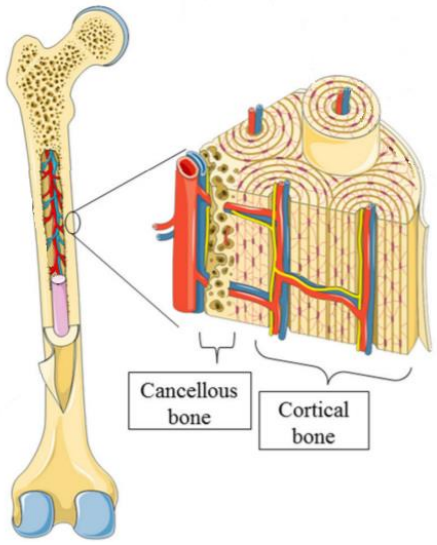

Figure 1. Schematic overview of the bone tissue with its macroscopical composition. Adapted from [197].

Even though the bone is known to have a high capability to regenerate, when faced with critical sized defects, it requires a tissue substitute capable of filling the gap. Currently, the most common used therapeutics are based on bone grafts, such as autografts (using bone collected from the patient's body) or allografts (using bone collected from a donor's body). However, these strategies present some drawbacks, including the amount of graft available, donor site morbidity or pain, and carrying major health risks for the patients[11]. These limitations boosted the development of synthetic materials capable of being used as bone graft substitutes[13] and offering better performances and more efficiency, in conjunction with superior mechanical, chemical and physical properties[12,25].

2. Biomaterials for bone tissue engineering

The term "biomaterials" is very broad and can be used to describe a wide variety of materials, from natural and synthetic materials alone to multiple components materials. These are often defined as materials that have been engineered to interact with biological systems, mainly for medical and clinical applications[26].

The first works related to bone tissue engineering began in the 70s and, since then, several researchers have been trying to develop new biomaterials with the composition and structure of bone in mind[1]. This evolution can be divided into three generations of biomaterials. A first one, in which the materials were normally bioinert, presented minimal interaction with other tissues and had the objective of replacing the missing tissue without, however, stimulating any cellular responses[27]. This includes metals (i.e., titanium), ceramics (i.e., alumina) or synthetic polymers (i.e., polymethyl methacrylate (PMMA**)**). Although these materials demonstrated great long-term integrity, the body often failed to adapt to them, which has led the scientific community to focus on materials that presented a more bioactive nature with the integration of engineered functionality to promote biological responses, the so-called second-generation biomaterials. It was possible to reach important milestones in this generation, with the development of materials with osteoconductive (conducts and allows bone tissue to grow on the surface or into the pores of the material [28]) and osteointegration (allows the bone to heal and maintains its function by forming bony tissue around the material [28,29]) properties, with some of them being degradable *in vivo*. Among these can be found bioactive glasses, natural and synthetic polymers (i.e., collagen, gelatine) or calcium phosphates, carbonates, and sulphates. This range of advanced properties and characteristics provided the foundation for the study of more and better biomaterials for bone tissue applications, thus giving rise to the beginning of the development of third generation biomaterials. This generation, still currently in progress, aims to induce specific biological responses through the addition of instructive substances to second-generation based biomaterials[30,31].

For the success of a synthetic bone graft applied in bone regeneration therapies, we can identify some essential characteristics (Figure 2): Biocompatibility (the material must be tolerated by the body, not causing an immune response); Bioactivity (the material must have the ability to bind to pre-existing bone and, more specifically, create a surface layer of HA through *in vivo* reactions in order to further increase binding to the host bone); Osteogenic (the material must be able to stimulate adult stem cells to differentiate into bone producing cells which can be achieved with the addition of active ions or other biological factors); Vascularization (the material should allow for the development of blood vessels and nutrient supply); Degradation (the material must have a degradation rate compatible with the rate of bone regeneration, without the formation of toxic products for the body); and lastly,

mechanical properties (the material must have bone-like mechanical properties in order to be able to withstand the *in vivo* conditions along with the rest of the bone)[32–34].

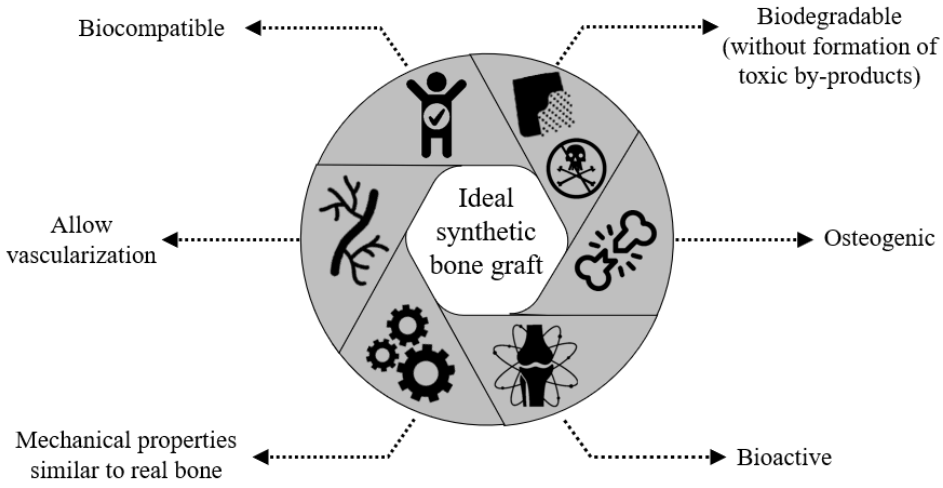

Figure 2. Schematic overview of the ideal synthetic bone graft properties.

During the constant process of searching for new types of materials, multifunctional materials capable of combining various properties and functions are gaining more and more prominence. In addition, the limitations observed in certain materials currently used further increased the need for a new approach to the problems. A possible solution lies in composites or hybrid materials[35].

2.1. Hybrid materials

Organic-inorganic hybrid materials are obtained through the combination of organic and inorganic building blocks at a molecular level. They can be defined as composites with organic and inorganic components profoundly mixed, presenting specific chemical bonds resulting in improved new properties and not only the sum of the properties of the materials individually[36]. Additionally, hybrid materials can also have different classifications based on different concepts. Considering the strength of bonds between the components, we can divide them into class I hybrids, with weak bonds (i.e., Van der Waals and hydrogen bonds

or weak electrostatic interactions), or into class II hybrids, with strong bonds (i.e., covalent, or ionic bonds)[37].

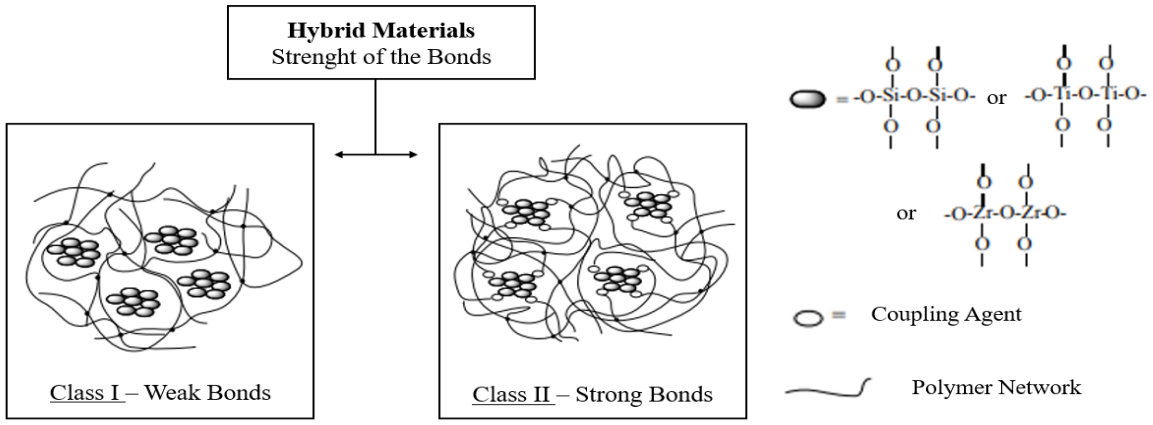

Figure 3. Scheme of the classification of hybrid materials with an example of morphological structures of Class I and II hybrid materials. Adapted from [54] .

Bone itself is considered to be a hybrid tissue composed of an organic part, collagen, and an inorganic part, mainly HA, with a highly hierarchical structure obtained through very complex processes encompassing cells, proteins, growth factors and hormones[38]. This inherent design of bone structure allows to achieve an ideal combination of desirable properties such as strength, toughness or lightness that can only be mimicked using a multiscale formation strategy[39].

2.2. Sol-gel method

The sol-gel process consists of a synthetic method used to develop organic-inorganic hybrid materials and, was first mentioned by Graham in 1864 in a work on silica sols[40]. All sol-gel based methods involve two distinct phases, the solution (sol) and the gelation (gel). On the one hand, the sol refers to a colloidal suspension of solid particles, while the gel represents the interconnected network between the solid particles that forms a continuous entity through a secondary (usually liquid) phase. The sol-gel technique allows both phases to be maintained and conserved[41].

The process is based on inorganic polymerization reactions using alkoxide precursors, $M(OR)_n$ (where M is a networking-forming element (i.e., Si, Ti, etc.) and OR is an alkoxy

group). The most used precursors are metal alkoxides, since they react readily with water. First, hydrolysis of the alkoxide precursor occurs, where a reactive hydroxy group (-OH) is introduced to the metal, forming reactive hydroxyl groups (M-OH). Then, the condensation of the hydroxyl groups occurs, with the formation of M-O-M units with the loss of water or alcohol molecules. The various condensation reactions lead to the formation of three-dimensional polymer networks [14,42–45].

The previous condensation reactions lead to the formation of aggregates which collide and form bonds between them, forming a larger aggregate and creating the gel. These links established between aggregates give rise to a continuous solid network and, as the gel becomes more aggregated, the greater is its viscosity[46,47]. The temperature used during this step (gelation temperature) has a direct impact on the final product obtained, and an increase in the porosity of the gel can be related with the increase of the temperature used[48]. Usually, a drying step is used to finalize the process, in order to remove any liquid by-products remaining in the pores which, consequently, leads to a shrinkage of the gel network[44,46].

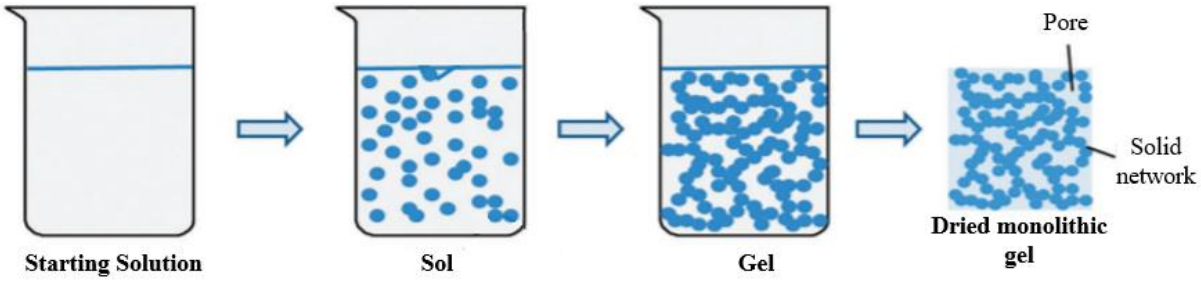

Figure 4. Scheme of steps involved in the preparation of materials by the sol-gel process. Adapted from [46].

This method has proved to be particularly useful, since it allows to obtain multicomponent materials with different configurations through direct fabrication, not requiring more expensive and complex processing technologies[49]. In addition to these advantages, the great diversity of materials that can be obtained through the sol-gel method make it an important technology for the synthesis of materials in various areas of research, from optics or electronics to biomaterials[41].

2.3. Organically modified silicates (ORMOSILs)

One of the most attractive features of the sol-gel process is the fact that it allows the preparation of various types of organic-inorganic hybrid materials that would be very difficult to obtain through other processes[50]. This new family of materials prepared by the sol-gel method is commonly referred to as ORMOSILs. The term was firstly used in 1984, when Phillip and Schmidt presented a work with the objective of combining two materials (organic and inorganic) in order to obtain a hybrid material that could be used as contact lenses with improved characteristics [45].

Since then, ORMOSILs have gained much interest from the scientific community, due to their wide range of applications, such as biomaterials, coatings, scaffolds, or drug delivery systems[35, 38,51,52]. Additionally, these modified silicates demonstrate great potential in the field of bone tissue engineering, as they are able to combine the bioactive properties of inorganic glasses with the mechanical properties of polymers through chemical bonding, achieving superior properties when compared to other materials[16,53].

Their formation starts with the inorganic component (i.e., silica) being incorporated into an inorganic network. Followed by the addition of the polymer (organic component) and the formation of inorganic chains around the polymer molecules[15,16] (Figure 5).

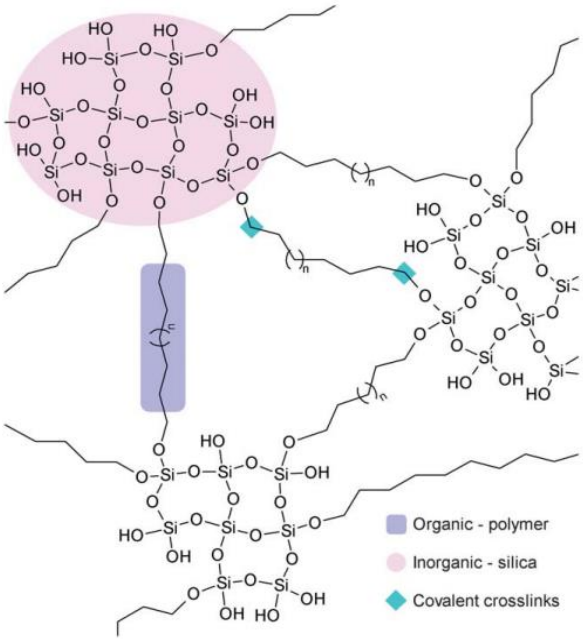

Figure 5. Scheme of a silica/polymer class II ORMOSIL[16].

The properties of the organic and inorganic components, as well as the conditions during the sol-gel process, will determine the final characteristics of the formed ORMOSIL[54,55]. One of the most studied types of ORMOSIL's are formed through the reaction between tetraethyl orthosilicate (TEOS) and polydimethylsiloxane (PDMS)[50].

2.3.1. PDMS- SiO_2 system

In 1985, two researchers, Wilkes[56] and Mark[57], carried out works with the objective of creating new materials through sol-gel processing containing silanol or alkoxysilyl terminated PDMS polymers and TEOS. PDMS is considered a polymeric material belonging to the subclass of elastomers and, its varied characteristics (i.e., chemical, and thermal stability[58,59], biocompatibility[60,61], flexibility[62], among others) make it one of the most used silicon-based polymers[62,63]. Its chemical structure consists of a (Si-O) backbone and repetitive (Si $(CH_3)_2$ O) units, which can be expressed as H_3[Si $(CH_3)_2$ O]*x* Si $(CH_3)_3$, where *x* represents the number of repetitive units that defines its molecular weight. The methyl group is represented by the (CH_3) and the (Si-O) represents the strength of the siloxane bonds which are responsible for giving the material its chemical and physical stability[63]. TEOS is an inorganic precursor and, usually, the principal network forming agent involved in sol-gel methods, with the capacity to form robust networks allied with easy control of the reactions through simple variations in the synthesis conditions (i.e., pH, temperature, additives)[41,64].

When subjected to hydrolysis, both components (PDMS and TEOS) give rise to very similar products, explaining the great chemical compatibility between the organic and inorganic parts of the hybrid materials formed by them. Additionally, similar chemical bonds (Si-O-Si) also allow for the control of hydrolysis and condensation reactions in order to obtain hybrid materials with high levels of hetero condensation, forming crosslinks between the organic and inorganic components[14] (Figure 6).

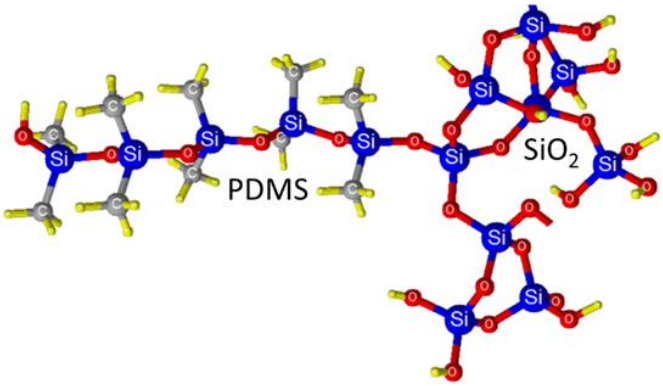

Figure 6. Hybrid structure of the PDMS-SiO_2 system with the organic (PDMS)-inorganic (SiO_2) bond. Adapted from[198].

We can describe the mechanisms that lead to formation of the PDMS-SiO_2 system through the hydrolysis of TEOS and PDMS and, subsequently, the co-condensation of Si-OH and $Si(CH_3)_2$-OH ending groups. The result is the formation of tetrafunctional Q^n(n=0,1,2,3,4) structural units (SiO_4), difunctional D^n (n=0,1,2) structural units ($(CH_3)_2SiO_2$) and the crosslinks between the two, $D_{(Q)}$ structural groups (n represents the number of bridging oxygen atoms surrounding Si). Additionally, the PDMS-OH can also undergo self-condensation reactions which leads to an increase in the molecular weight of the PDMS in the system. TEOS is used as a crosslinking agent in this system to prevent the growth of PDMS chains and, its self-condensation occurs simultaneously during all previous reactions[65]. The schematic reaction mechanisms of silanol-terminated PDMS and TEOS are presented next.

TEOS Hydrolysis:

$$Si(OC_2H_5)_4 + nH2O \rightarrow Si(OH)_n(OC_2H_5)_{4-n} + nC2H_5OH \quad \textbf{(1)}$$

Si-OH + PDMS-OH co-condensation:

$$\equiv Si\text{-}OH + HO\text{-}[Si(CH_3)_2\text{-}O\text{-}]xH \rightarrow \equiv Si\text{-}O\text{-}[Si(CH_3)_2\text{-}O\text{-}]ySi\equiv + \equiv Si\text{-}O\text{-}[Si(CH_3)_2\text{-}O\text{-}]ySi\text{-}OH + H_2O \quad (x > y) \quad \textbf{(2)}$$

Si-OH self-condensation:

$$\equiv Si\text{-}OH + OH\text{-}Si\equiv \rightarrow \equiv Si\text{-}O\text{-}Si\equiv + H_2O \quad \textbf{(3)}$$

PDMS-OH self-condensation:

$HO\text{-}[Si(CH_3)_2\text{-}O\text{-}]xH + HO\text{-}[Si(CH_3)_2\text{-}O\text{-}]yH \rightarrow HO\text{-}[Si(CH_3)_2\text{-}O\text{-}]zH + [Si(CH_3)_2\text{-}O\text{-}]_4$
(*cyclic specie*) + H_2O ($x,y < 1z$) **(4)**

The previous reactions will result in a hybrid material with controlled characteristics and properties. In general, the polymerization process that occurs in the formation of the hybrid material is quite complex, causing the sol-gel process to be fundamentally affected by the reaction conditions (i.e., pH of the medium, temperature, solvent composition, or molar ratio of the reactants)[54,55].

One important factor is the H_2O/TEOS molar ratio, *r,* and, when water content increases, TEOS hydrolysis reactions are accelerated at the expense of the condensation rate allowing the co-condensation reactions with PDMS-OH to occur[41]. Additionally, the hydrolysis-condensation reaction rates are also affected by the type and concentration of catalysts, either an acid or a base. When the synthesis occurs under acidic conditions, the hydrolysis rate of TEOS is promoted and, consequently, more PDMS will be incorporated into the system. The TEOS condensation rate increases with pH and, increased *r* values lead to an increase of hydrolysis rates at any particular pH[66–68].

In this specific hybrid system, the role of the acid content is even more complex since it also can change the siloxane distribution through the hydrolyzation of Si-O-Si bonds. It is also important to note that under extreme pH values a degradation of the polymer can occur, being necessary the usage of adequate pH values to guarantee the maintenance of its integrity and molecular weight[15,69,70].

Another important factor is the TEOS/PDMS ratio used in the reactions, which allows the control of certain physical properties of the final material, such as its elastic modulus or stiffness. Depending on the amount (and the molecular weight) of PDMS used, the result could either be a flexible or brittle material[14] and, it is possible to obtain hybrid materials with “rubbery” like behaviour when large amounts of TEOS are used[71].

The synthesis of hybrid materials using the sol-gel method has several advantages, such as mild processing conditions, high levels of purity and homogeneity of the final products, low temperatures required and possible modification of the synthesis conditions. Thus, the incorporation of the organic component in an inorganic network and the interactions between

both components, allows the obtention of hybrid materials with desirable morphology, size, and multifunctional properties[72,73].

In order to improve the properties of the PDMS-SiO_2 system, mainly at the biological level, it may be necessary to introduce additional components to the system. This need, combined with the existing knowledge regarding the positive effects of certain metal ions (i.e., calcium, strontium, phosphorous, silicon, zinc, etc.) in the metabolic processes involved in tissue formation, demonstrates the great potential of these ions to enhance osteogenesis and, lead to better overall bone regeneration when incorporated into the composition of biomaterials[74–76]. Some important examples of well-studied components used for bone therapies are calcium or strontium. Calcium (Ca) ions are already known to be involved in the growth and maintenance of bone tissue, contributing to the processes of osteoinduction and osteoconduction that lead to bone regeneration[77,78]. Strontium (Sr) is responsible not only for increasing osteogenic activity, making it a potential bone formation promoter, but also for inhibiting osteoclast activity[79,80]. Its numerous advantages at the bone tissue level make it an object of great scientific interest, being already used as a therapy for osteoporosis and prevention in the form of strontium ranelate[81].

3 Resveratrol

Resveratrol (3,5,4'-trihydroxystilbene; RES) is a stilbene polyphenol, with two phenol rings linked to each other by an ethylene bridge[82,83]. Its chemical structure has two conformations, *cis*- and *trans*-resveratrol (Figure 7), with the *trans* form being dominant in terms of prevalence and presenting several beneficial biological activities[84]. The *cis*-isomerisation usually occurs when the *trans*-isoform is subjected to solar or ultraviolet radiations [85] at wavelengths of 254 [86] or 366 [87] nm.

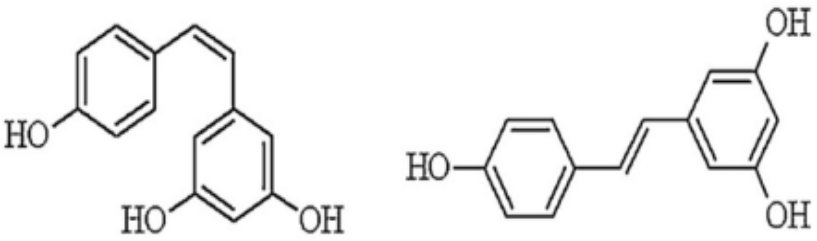

Figure 7. Chemical structure of cis-(left) and trans-(right) RES [82].

The pharmacological interest in *trans*-RES (T-RES) initially emerged from studies that identified its presence in wine[88], and related the consumption of this substance with beneficial health effects. A well-known example is the so-called "French Paradox", in which it was possible to relate the consumption of red wine (known to contain large concentrations of T-RES) with a low mortality rate caused by cardiovascular diseases in the French population despite its high consumption of saturated fats[89]. Since then, T-RES has been the subject of several studies that highlight its wide range of biological properties, including antioxidant, cardioprotective, neuroprotective, anti-inflammatory, or anticancer/antitumoral activities[90,91]. These properties make T-RES a very versatile molecule, with therapeutic applications in various diseases such as obesity and diabetes[92,93], cancer[94,95] or cardiovascular[96,97] and neurodegenerative[98,99] diseases.

Its wide range of biological and pharmacological properties, including antitumor and cancer preventive potential, make this pharmacological agent a tool for preventing and treating bone cancer[100–102].

3.1 Resveratrol in bone therapies

Several studies show that RES can be effective on bone healing and regeneration, due to its osteogenic and osteoinductive properties[103,104]. Furthermore, their benefits on more specific cases of bone related diseases have also been evaluated, showing very promising results.

Wang *et al.* conducted a study with the aim of determining the protective effects of RES on a rat model of osteoporosis and examine the associated mechanisms of its action. The

evidence showed that RES treatment significantly increased the bone mineral density (BMD, measurement commonly used to diagnose osteoporosis) in rats[105]. Another study, by Wong *et al*., had the objective of analyzing the effects of RES in the BMD in women with postmenopausal osteoporosis (which is caused by an estrogen deficiency). The results showed a significant improvement in BMD of the lumbar spine and femoral neck (which are considered critical sites outlined by the International Society for Clinical Densitometry for diagnosing osteoporosis) that was partially explained by the effects of RES in the estrogenic pathway, exerting positive effects on bone health of postmenopausal women[106].

Additionally, its wide range of antitumor and cancer preventive potential, make this pharmacological molecule a tool for preventing and treating bone cancer, such as osteosarcoma[100–102]. Zou *et al.* assessed a total of 14 botanical extracts aiming to identify potential novel molecules for the treatment of osteosarcoma. RES showed significant anti-osteosarcoma activities in blocking cell proliferation and activating apoptosis[107]. In another study performed by Peng *et al.*, the effect of RES on osteosarcoma stem cells was examined and, it was demonstrated that inhibited cell viability, self-renewal ability and tumorigenesis of osteosarcoma cells leading to significant osteosarcoma stem cell elimination effects after the treatment, with no significant inhibition effects to normal osteoblast cells. The evidence showed that RES can be considered an effective osteosarcoma stem cell targeting agent for inhibiting disease progression and treatment[108]. More recently, Xu *et al.* used a MG-63 osteosarcoma cell culture model to access the chemotherapeutic effect of RES. The results suggested that RES was able to block cell proliferation, migration, and invasion, and activate apoptotic cell death in this osteosarcoma cell line[109]. These findings support the use of RES in the clinical treatment of patients with osteosarcoma.

Furthermore, RES has also been shown to have effects in bone cancer pain (BCP). BCP is one of the most common pains in patients with malignant cancers showing strong effects in the patient's quality of life[110]. Lux *et al.* studied the antinociceptive effect of single and repeated doses of RES in a BCP model and concluded that both types of treatments induced antinociceptive effect in the BCP model, while also improving functionality[111]. Another study from Zhu *et al.*, also showed that RES could reverse pain behavior in BCP model rats[112]. These studies demonstrate the potential benefits of using RES as a therapeutic treatment during BCP states.

3.2 Resveratrol drug delivery systems

Despite demonstrating enormous therapeutic potential and several health benefits, RES presents some pharmacokinetic limitations that restrict its clinical and pharmacological applications. The most important disadvantageous properties are its low water solubility that makes the distribution throughout the body dependent on its ability to bind to plasma proteins, which consequently affects its bioavailability[113–115]; its short biological half-life[116,117] and extensive and fast metabolism and elimination which, once again, leads to its low bioavailability[118]; and its chemical instability due to high photosensitivity and tendency to suffer oxidation[119]. Additionally, also high temperatures, changes in pH and certain enzymes can lead to chemical degradation of RES, affecting its properties[120,121]. Conventional drug delivery solutions contain RES in an appropriate dosage form, usually as a tablet, capsule, or solution[122]. However, this approach is not able to overcome the limitations found, since, after an oral dose, the metabolic pathways only leave small amounts of RES in the blood, resulting in very low bioavailability in the target tissues[123]. Thus, during the last decades novel drug delivery systems (DDS) have emerged to suppress these problems, using an interdisciplinary strategy that combines materials science, chemistry, pharmaceuticals, and molecular biology [124].To be considered ideal, the delivery system must be able to transport and deliver the therapeutic molecule/agent to the target site (organ/tissue) in the body, so that it acts promptly and maintains its desired drug concentration and effect[125].

Through the years, researchers developed various DDS aiming to increase RES absorption and, not only, overcome its solubility, stability, and bioavailability challenges, but also protect against light, oxygen, and other environmental factors that can compromise its properties[119,126]. Some examples of materials proposed to solve these limitations include cyclodextrin complexes[127–129], liposomes[130–132], polymeric micelles[133] or nanoparticles[134,135]. Nonetheless, these DDS are far from perfect, presenting limitations such as low stability, insufficient drug loading, the need for organic solvents and the expensive production costs[136].

On the other hand, inorganic systems such as mesoporous silica nanoparticles (MSNs) have superior properties when compared to other nanocarriers, making the interest in its use as a support for the encapsulation and delivery of RES grow immensely in recent years.

Some of these properties are their high surface area and pore volume, which allows for high drug loading capability, easy surface functionalization, due to the silanol functional groups available for chemical modifications, controllable morphology such as the mesopore sizes and pore/shape connectivity and good biocompatibility[137,138]. Additionally, one of the most important and interesting features of MSNs is their ability to encapsulate both hydrophilic and hydrophobic molecules with similar loading efficiency[139,140]. Since many of the pharmacological agents are hydrophobic in nature (as is the case with RES[82]), these systems show great potential to overcome the solubility challenges of this type of substances.

With these characteristics of silica nanoparticles in mind, there are already several works that report the encapsulation of RES in silica-based materials that share the notion that silica provides a support suitable for the stabilization of T-RES with controlled release, ability to protect the molecule against degradation and enhance its bioavailability, making these systems a good DDS for RES, with potential for various clinical applications[141–146].

III. Experimental Procedure

1. Applied chemicals

Tetraethyl orthosilicate (TEOS, ≥ 99.0%), polydimethylsiloxane silanol terminated (PDMS, 550 g/mol average molecular weight), phosphate buffered saline pH 7.4 (0.01 M PBS, 25 ºC) packets and the dialysis cellulose tubing membrane (3 kDa cut off) were obtained from Sigma-Aldrich (St. Louis, MO, USA). Isopropyl alcohol (IPA, ≥ 99.8%) from Fischer Chemical (Loughborough, UK). Hydrochloric acid (HCl, 25%) was purchased from Panreac Quimica SLU (Barcelona, Spain) , *trans*-resveratrol (T-RES, 99%) from Tokyo Chemical Industry (TCI Europe N.V., Zwijndrecht, Belgium) and ethanol absolute from VWR (Radnor, PA, USA). Ultrapure water (Mili-Q®) was used in all experiments. All the chemicals referred were used as received without further purification.

2. Samples preparation

The samples have been prepared through a sol-gel process, at room temperature, by adding IPA, PDMS, H_2O, HCl and TEOS using the molar ratios shown in Table 1.

Table 1. Composition of the PDMS-SiO_2 samples

Notation	**Composition (molar ratio/TEOS)**			
	IPA	**PDMS**	**H_2O**	**HCl**
M0C0-I	3.1	0.16	6.3	0.2
M0C0-II	3.1	0.16	6.3	0
M0C0-III	3.1	0.16	10.8	0.2
M0C0-IV	3.1	0.16	6.3	0.4

Firstly, IPA, PDMS and H_2O were added in the respective order, always under continuous stirring, using a magnetic stirrer. Then, the medium was acidified by the addition of HCl, that was used as a catalyst to the hydrolysis/condensation process, and TEOS. The solution remained under the magnetic stirrer for about 30 min. After stirring, the final

suspension was placed in a petri dish and kept at room temperature for 24 h for aging, remaining liquid and transparent. Later, the samples were placed in the oven at 60ºC for 24 h. Finally, in order to remove all solvents from the samples, they were placed for 1 h in an oven at 150 ºC. The experimental procedure used to prepare the PDMS-SiO_2 system hybrid materials is shown in Figure 8.

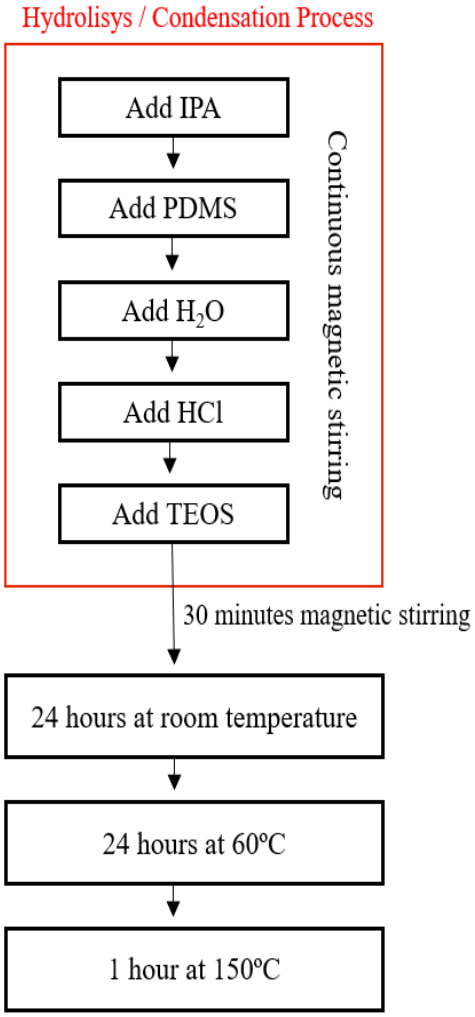

Figure 8. Experimental protocol used to prepare the PDMS-SiO_2 samples.

Figure 9 shows the samples after the drying steps, where we can see that three of the samples (M0C0-I, M0C0-III and M0C0-IV) resulted in white opaque and homogeneous monoliths. Sample M0C0-II resulted in a transparent non-homogenous material, indicating

that the lack of HCl affected the hydrolysis/condensation processes and, consequently, the final material, causing it to not be used in the following steps of the work.

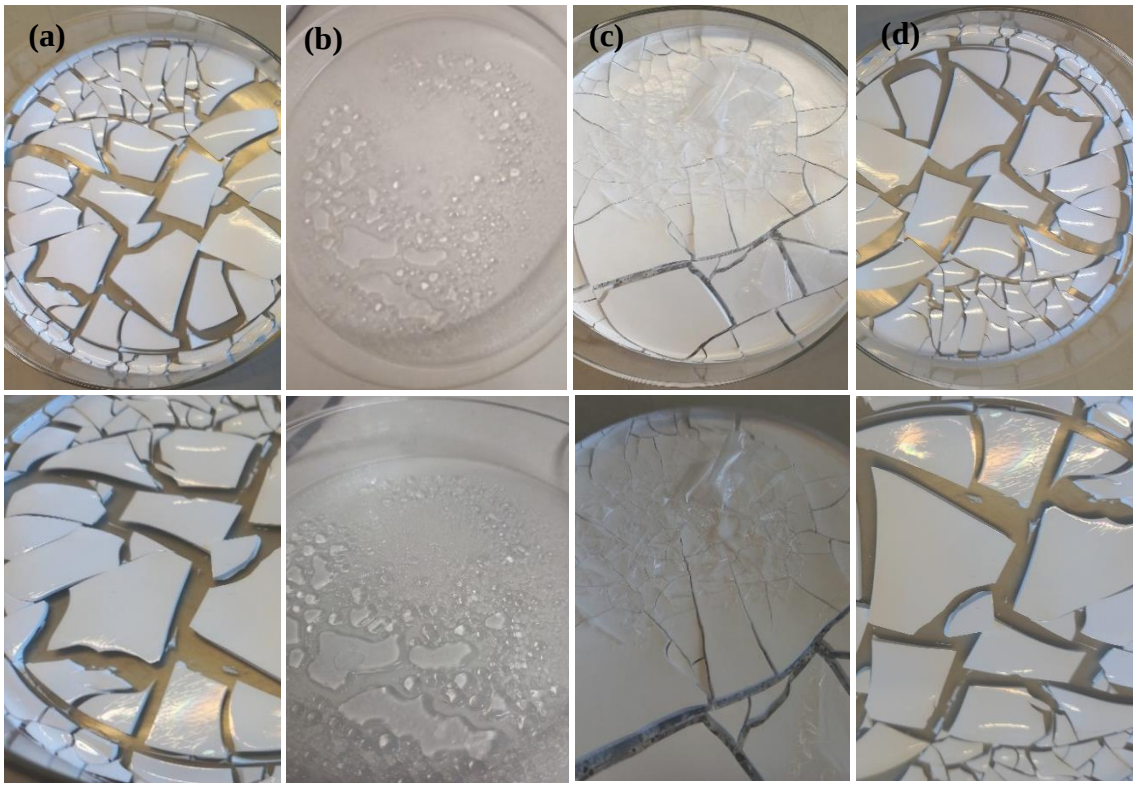

Figure 9. PDMS-SiO2 samples after being dried: (a) M0C0-I; (b) M0C0-II; (c) M0C0-III; (d) M0C0-IV.

3. RES-loaded samples preparation

RES loading was performed using the rotary evaporation technique [144,147,148]. In a typical procedure, 160 mg of RES were dissolved in 30 mL of ethanol and the solution was placed in an ultrasonic bath for 4 min. Afterwards, 200 mg of the PDMS-SiO_2 material was added to the solution and the dispersion was placed in the ultrasonic bath for 10 min. The solvent was then evaporated at 50 °C in a rotary evaporator (Buchi) until all ethanol was removed, to obtain the RES-loaded PDMS-SiO_2 samples (-RES). The final solids were scratched off from the round bottom flask and stored at room temperature, protected from light with aluminium foil.

4. Physicochemical characterization

The samples obtained by the methods described above were characterized at a structural and microstructural level. The samples were first pulverized in an agate mortar in order to create thin powders. Next, the characterization techniques that were performed on the materials will be briefly described.

4.1. X-Ray Diffraction (XRD) analysis

XRD is a non-destructive technique used to structurally characterize materials, providing information on several structural parameters such as structures, phases or preferred crystal orientations (texture). The analysis is based on the interaction of monochromatic X-rays directed towards the sample, which generates a constructive interference (and a diffracted ray) when the conditions are compatible with the Bragg's Law[149], which is given bellow:

$$n\lambda = 2d \sin\theta \quad \textbf{(5)}$$

where n is an integer, λ is the wavelength of the incident X-ray beam, d represents the distance between near atomic planes or d-spacings and θ marks the angle of the incidence X-ray. This law relates the wavelength of electromagnetic radiation to the diffraction angle and the lattice spacing in a crystalline sample. Then, the diffracted X-rays are detected, processed, and counted, and, when scanning the sample over a specific range of 2θ angles, all possible directions of diffraction of the lattice should be collected due to the random orientation of the powdered material[150–152].

For the analysis, a Pan Analytical -X'pert-PRO diffractometer equipped with a copper anode (Cu) was used, which operates with a current of 40 mA and a voltage of 45 kV, emitting a $K\alpha_1$ radiation of λ=1.540598 Å and $K\alpha_2$ of λ=1.544426 Å. The spectra were recorded through a continuous scan from the smallest possible angle, which was 2θ=2°, up to 2θ=60°, with a step size of 0.0263° and a step time of 96.39 seconds, at room temperature.

XRD analysis was important in this work because it provided information about the amorphous character of the hybrid material. Since each material has its unique diffraction beam, the identification of the crystallographic phases can be done by comparing the

diffracted beams with the reference database in the JCPDS (Joint Committee on Powder Diffraction Standards) library.

4.2. Fourier Transform Infrared (FT-IR) spectroscopy

FT-IR spectroscopy is an analytical nondestructive technique used to study the chemical bonds or molecular structure of different materials. The analysis uses infrared (IR) radiation to scan samples and the collected data is converted to the desired result through a well-known mathematical technique called Fourier Transformation (FT). This conversion is carried out by a computer program, which then presents the user with the desired spectral information for analysis[153,154].

Each chemical bond vibrates at a characteristic frequency and, when exposed to IR radiation, these absorb the radiation at frequencies that match their vibration modes. Thus, the spectrum produced by measuring the radiation absorption frequency can be used to identify functional groups and compounds in the samples, since the intensity and position of each peak corresponds to the vibrational mode of a specific chemical bond[153,155,156].

In this work, FT-IR spectra were collected on a Mattson–7000 spectrometer, 128 scans were collected per sample over the range of 4000 to 300 cm^{-1} at a resolution of 2.0 cm^{-1}. The samples were prepared using the KBr technique in which, prior to the analysis, each powder sample was mixed and grinded in an agate mortar with a small amount of potassium bromide (KBr) and pressed to produce the disks used in the analysis.

4.3. Specific Surface Area by the Brunauer-Emmett-Teller (BET) method

The specific surface areas (SSA) of the samples were determined using the Brunauer-Emmett-Teller (BET) method, which can be described as a mathematical way of analyzing the adsorption isotherms of non-reactive nitrogen gas. The technique requires the placement of a known quantity of an inert gas, normally nitrogen, into the sample, which makes the particles adsorb a molecular layer of nitrogen on the surface of the material. After the formation of the adsorbed layers (when saturation pressure is reached), is removed from the atmosphere containing nitrogen and heated so that the adsorbed nitrogen particles are

released from the material surface. The data collected is then quantified and displayed as a BET isotherm that represents the amount of adsorbed gas as a function of relative pressure:

$$p/p^0 \quad \textbf{(6)}$$

where p^0 is the saturation vapor pressure of the adsorbed substance at the temperature at which the assay is performed. The amount of the adsorbed gas on the adsorbent material can be correlated with its surface area, which is defined as the surface area of a solid particle per unit mass, usually expressed in m^2/g[157].

According to the International Union of Pure and Applied Chemistry (IUPAC), there are six types of isotherms obtainable through the BET method, each one corresponding to a specific adsorption mechanism. The different types are presented in Figure 10 and the corresponding descriptions are summarized next[158,159].

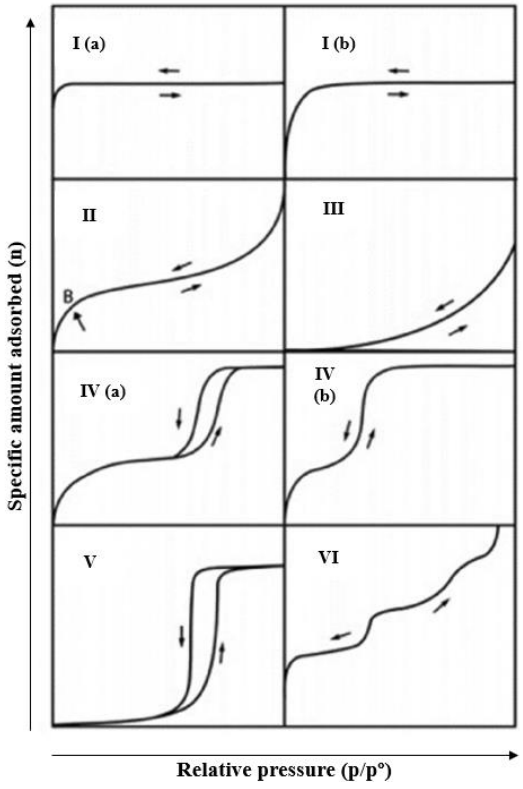

Figure 10. Types of gas absorption isotherms, according to IUPAC's classification.

Type I. Microporous materials with relatively small external surfaces. Can be divided into two patterns: I (a) for materials with micropores below ≈1 nm of width; I (b) for solids with both wider micropores and narrow mesopores (<≈2.5 nm).

Type II. Nonporous or macroporous materials. Point B indicates the stage at which we have a complete monolayer coverage and when the multilayer adsorption starts.

Type III. Nonporous materials with weak interactions between the adsorbent and the adsorbate.

Type IV. Common in mesoporous materials. Has two possible patterns, both related to the width of the pores: IV (a) for when the size of the pore's width is higher than the critical width; IV (b) for pores with smaller widths.

Type V. Micro and mesoporous materials. The observed shape at over low relative pressure ranges is similar to type III, which can be attributed to the weak adsorbent–adsorbate interactions. At higher values of relative pressure hysteresis similar to type IV (a) can be observed.

Type VI. Materials with uniform nonporous surfaces with multilayer adsorption mechanisms. The pattern observed is in the form of a stepwise curve which depends on the material, gas, and temperature used.

In isotherms from type IV and V, a phenomenon called hysteresis can occur, in which the adsorption curve doesn't coincide with the desorption curve. Figure 11 exemplifies four possible hysteresis, where each one represents a type of pore shape: type H1 is normally associated porous materials with spherical particles and rigid agglomerates; type H2 is related to materials with bottle-shaped pores; type H3 corresponds to particles with plaque morphology, developing slit-shaped pores; and, lastly, type H4 is associated with slit-shaped and narrow pores[160].

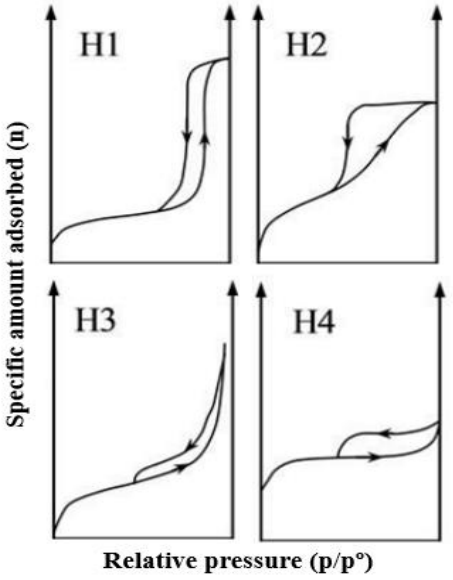

Figure 11. Different types of hysteresis, according to IUPAC's classification

The analysis in this work was performed on a Quantachrome - Autosorb IQ2 equipment. Previous to the analysis, the samples were degassed at 150 ºC for 12 h and cooled until room temperature.

4.4. Scanning Electron Microscopy (SEM)

Scanning electron microscopy (SEM) is a commonly used advanced technique for materials characterization. SEM uses a focused beam of electrons that, once emitted, strikes the surface of the sample, and gives rise to secondary and backscattered electrons. The detection of these emitted electrons is responsible for the formation of the sample image obtained. It can be regarded as an effective technique for the analysis of organic and inorganic materials, providing high resolution images from a nanometer to a micrometer scale with a relatively large depth of field, giving information on the morphology, topology, and surface porosity of the samples[161–163].

This technique was used to perform a microstructural analysis of all the samples and was carried out using the Hitachi microscope SU - 70 model (with an acceleration voltage of 10 KV). The samples were prepared for the analysis trough the fixation of the powder samples in an aluminium sample holder with double-sided carbon tape.

4.5. Thermogravimetric Analysis (TGA)

Thermal methods are based on the characterization of a system (element, compound, or mixture) by measuring changes in physicochemical properties at elevated temperatures as a function of increasing temperature. One type of thermal method is the TGA, in which changes in weight are measured as a function of increasing temperature[164].

TGA was employed to access the amount of RES loaded on the material, in a Hitachi STA300 equipment with a heating rate of 5 ºC/min (temperature range 30-800 ºC), under a nitrogen-oxygen atmosphere (3:1).

5. *In vitro* solubility and release assays

5.1. Solubility studies

Solubility studies were performed using PBS at pH 7.4. The suspensions were prepared by dispersing 10 mg of the RES loaded materials in 10 mL of PBS. The samples were kept under continuous but gentle stirring at 37 °C and protected from light for 24 h. The study was also performed using free RES for comparison purposes.

UV–VIS absorption spectra of each sample were recorded in the range of 200–500 nm with 0,48 nm resolution using a UV/VIS spectrophotometer (GBC UV/VIS 918) at room temperature. Maximal RES absorption in aqueous solution at 304 nm was used to identify and quantify the RES concentration of the removed samples (r2 = 0.99996, Figure sm2, Supplementary material).

5.2. *In vitro* release studies

In vitro release studies were performed using PBS at two different pH values, 7.4 and 5.2. The suspensions were prepared by dispersing the RES loaded M0C0-IV material (equivalent to 2 mg of free RES) in 1 mL of PBS, introduced into a dialysis membrane (with

a 3.5 kDa molecular weight cut-off) and immediately immersed in 49 mL of PBS. The samples were kept under continuous but gentle stirring at 37 °C, protected from light. At predetermined time intervals 1 mL of the sample was withdrawn and immediately replaced with an equal volume of PBS to maintain sink conditions. For comparison, the test was also performed using free RES. The process used to identify and quantify the RES content in each sample is similar to the one used in the previous solubility studies (r2 = 0.99996 and r2 = 0.9992 for pH 7.4 and 5.2, respectively; Figure sm1, Figure sm2, Supplementary material). The cumulative release percentage of RES was calculated as follows:

$$Cumulative\ release\ (\%) = \frac{Volume\ of\ sample\ withdrawn\ (mL)}{Bath\ volume\ (mL)} \cdot P(t-1) + Pt \qquad \textbf{(7)}$$

where *Pt* corresponds to the percentage released at the time *t* and *P(t – 1)*, the percentage released previous to time *t*. The data presented in the release curves are an average of replicates.

6. Cell studies

6.1. Reagents

Dimethyl sulfoxide (DMSO; ≥99.7%) and 3-(4,5 dimethyl-2-thiazolyl)-2,5-diphenyl tetrazolium bromide (MTT; 98%) were purchased from Sigma-Aldrich (St. Louis, MO, USA). The MG-63 human osteosarcoma cell line was purchased from American Type Culture Collection (ATCC, Rockville, MD, USA). Dulbecco's Modified Eagle's Medium, fetal bovine serum (FBS), l-glutamine, and fungizone (250 U mL^{-1}) were obtained from Pan Biotech (Aidenbach, Germany), and penicillin–streptomycin (10,000 U mL^{-1}) from Grisp (Porto, Portugal). Trypsin–ethylendiaminetetraacetic acid EDTA (0.25% trypsin and 1 mM EDTA) was purchased from Gibco, Life Technologies (Grand Island, NY, USA).

6.2. Cell culture and preparation of the samples

Samples M0C0-IV and M0C0-IV-RES were incubated in medium, under continuous but gentle stirring at 37ºC for 48 h. After the 48 h, the extracts were centrifuged, and used to prepare the different concentrations used in the cell viability assay.

MG-63 cells were aseptically grown in Dulbecco's Modified Eagle's Medium, supplemented with 10% (FBS, 2 mM l-glutamine, 1% penicillin–streptomycin (10,000 U mL^{-1}), and 1% fungizone (250 U mL^{-1}) at 37 ◦C in a humidified atmosphere with 5% CO_2. After 24 h, cells were observed for confluence and morphology using an inverted phase-contrast Eclipse TS100 microscope (Nikon, Tokyo, Japan). Sub confluent cells were trypsinized with trypsin–EDTA (0,25% trypsin and 1 mM EDTA) when monolayers reached 80-90% confluence.

6.3. *In vitro* cell viability assay

Cell viability was determined by the colorimetric MTT assay. This method is based on the conversion of MTT into purple formazan crystals by living cells, thus determining their mitochondrial activity. Since, for most viable cells, mitochondrial activity remains constant, when there is an increase or decrease in the number of viable cells, this value will be linearly related to the mitochondrial activity. Giving its ease of use, this assay is commonly used to measure the in vitro cytotoxicity of several drugs at different concentrations on cell lines[165,166].

MG-63 cells were seeded in 96-well plates at 4000 cells $well^{-1}$ for 24 h of exposure at 37ºC in a 5% CO_2 humidified atmosphere. After 24 h, the medium was replaced with fresh medium containing: (a) pristine M0C0-IV extract (0, 25, 50, 100, 200, and 400 µg mL^{-1}), (b) RES loaded M0C0-IV extract (0, 25, 50, 100, 200, 300 and 350 µg mL^{-1}), and (c) bulk RES (0, 50, 75, 150, 300, 450 and 500 µM). Cell exposed to the control medium were used as a negative control, and cell viability was measured after 24 h. At the end of the incubation time, the wells were emptied and washed with PBS to remove remaining particles, and then fresh medium (100 µL) was placed in each well. After that, 50 µL of MTT (1 g L^{-1} in PBS) was added to each well and incubated for 4 h at 37 ◦C in a 5% CO_2 humidified atmosphere.

Following, the culture medium with MTT was removed and replaced by 150 µL of DMSO and placed in an orbital shaker (for 2 h, protected from light) for formazan crystal solubilization. The samples absorbance (Abs) was measured with a BioTek Synergy HT plate reader (Synergy HT Multi-Mode, BioTeK, Winooski, VT, USA) at 570 nm. The percentage of viability was calculated using Equation (8).

$$Viability\ (\%) = \frac{Abs(570)\ of\ samples}{Abs(570)\ of\ negative\ control} \cdot 100 \quad \textbf{(8)}$$

IV. Results and Discussion

The results obtained from the various characterization techniques used will be discussed and analyzed in detail in this chapter. Firstly, the PDMS-SiO_2 samples will be characterized, followed by the characterization of the RES loaded samples and the comparison of both the results in order to understand how RES was loaded on the materials.

1. Characterization of PDMS-SiO_2 samples

1.1. XRD analysis

XRD analysis was performed on each PDMS-SiO_2 sample (M0C0-I, M0C0-III, and M0C0-IV) to confirm its amorphous character, and the results obtained are presented in Figure 12. Observing the graphic, it is possible to note that there is one broad and undefined peak around a specific 2θ angle, approximately at 6º, which indicates the amorphous nature of the samples.

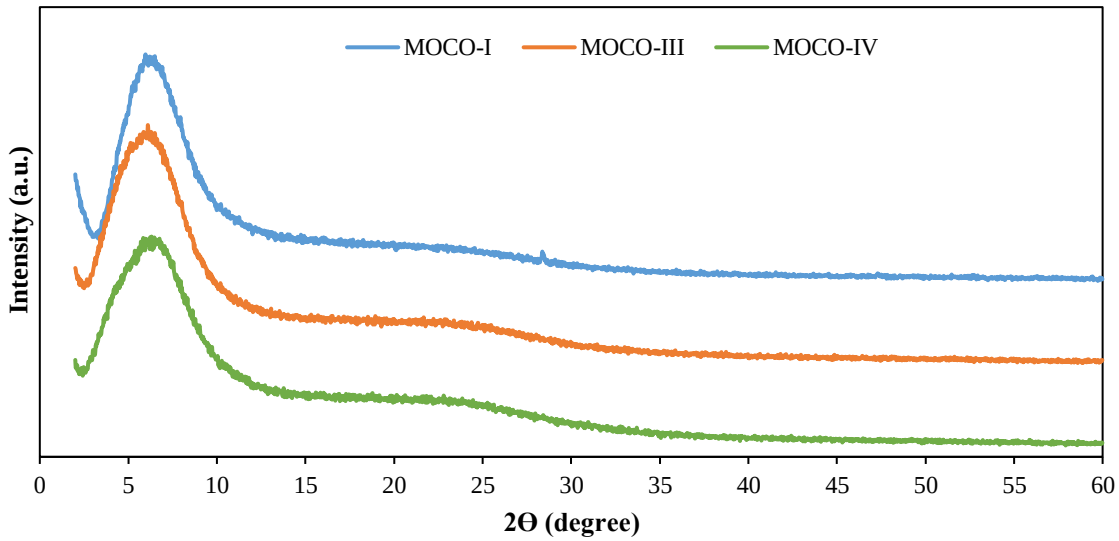

Figure 12. XRD spectra of the PDMS-SiO_2 samples.

According to the Braggs Law, by determining the 2Θ angle of each sample, it is possible to determine the distance in Å. Table 2 presents the values for the previous parameters. The

difference in the angle between each composition is minimal, always around the 6º corresponding to calculated distances between 14.0 and 14.7 Å. These values are approximated to the value of 13 Å previously calculated by Brus and Dybal for a similar hybrid system[167].

Table 2. Values of the maximum angle and distance between inorganic centres of the PDMS-SiO_2 samples.

Sample	2Θ (Degree)	Distance (Å)
M0C0-I	6.021	14.7
M0C0-III	6.126	14.4
M0C0-IV	6.310	14.0

1.2. FT-IR spectroscopy analysis

FT-IR studies were performed to study the chemical bonds present in the different PDMS-SiO_2 hybrid samples, and the data acquired is located in the spectral range of 300-4000 cm^{-1}. All the samples analyzed demonstrated IR bands in the region of 350-4000 cm^{-1}, which is compatible with previous literature concerning the characteristic bands observed for PDMS and silica hybrid systems similar to the one in this work[65,168–174].

Figure 13 shows the FT-IR spectra of all the samples in the spectral range of 1500-4000 cm^{-1} and 1500-300 cm^{-1}. As can be seen, the incorporation of PDMS within the network was confirmed by the presence of the asymmetric and symmetric CH_3 deformation bands at 1408 and 1265 cm^{-1} respectively, together with the asymmetrical C-H stretching at 1968 cm^{-1}. The formation of the inorganic network composed of Si-O-Si bonds was confirmed by the appearance of typical asymmetric Si-O-Si stretching vibrations at 1090 cm^{-1}, symmetric vibrations of Si–O-Si bonds at 805 cm^{-1} and Si-O-Si vibration in 4-fold siloxane rings at 555 cm^{-1}. The presence of bands at 850 cm^{-1} and 430 cm^{-1} are due to the presence of crosslinked SiO_2 (Q units)- PDMS (D units) structures, thus forming D-Q bonds and confirming the formation of hybrid structures with bonds between the organic and inorganic parts of the material. The previous values are similar to values already observed in previous works[173,175–177]. In samples M0C0-I and M0C0-IV, the peaks observed around 430 cm^{-1} are divided into

two small and not defined peaks, this is due to the fact that the samples were prepared using less H_2O which led to the formation of more hybrid bonds (D-Q structures). In the other hand, sample M0C0-III, prepared with a higher amount of water, presents a more defined peak at 430 cm^{-1}, indicating the presence of less hybrid bonds and more long chains[65].

The band observed around 3430 cm^{-1} can be attributed to the hydrogen-bonded silanol groups with absorbed molecular water, and the peak at 1625 cm^{-1} corresponds to O-H bending in the molecular water [172,177]. The peaks at 2360 cm^{-1} are related with the asymmetric stretching vibration of gas-phase CO_2 originated from ambient air absorption in the optical path outside the FT-IR cell[178].

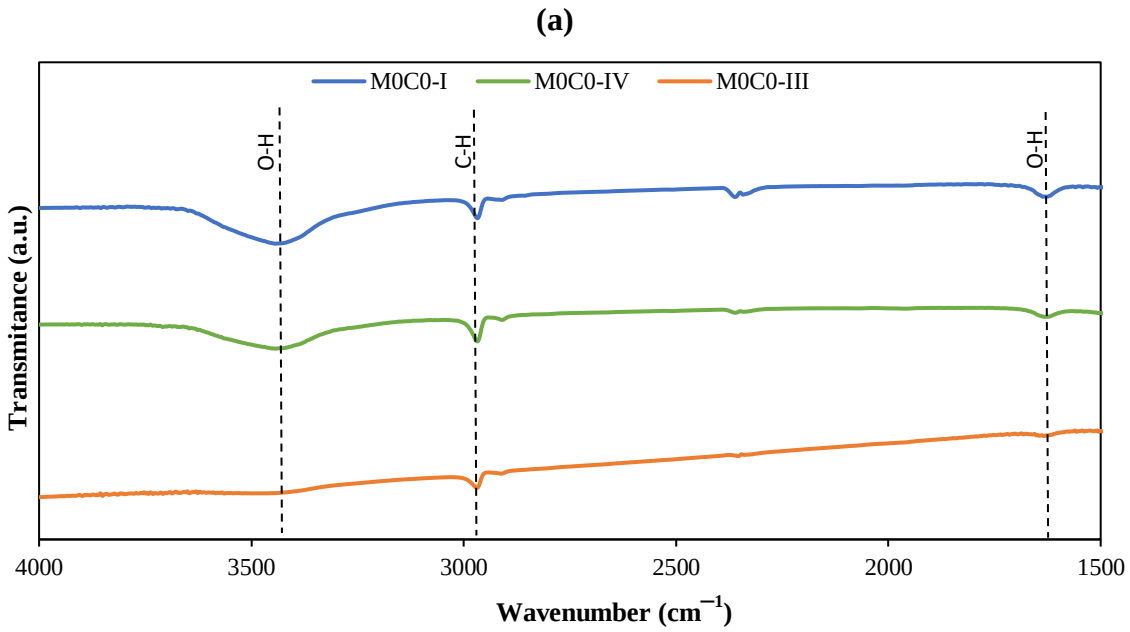

(b)

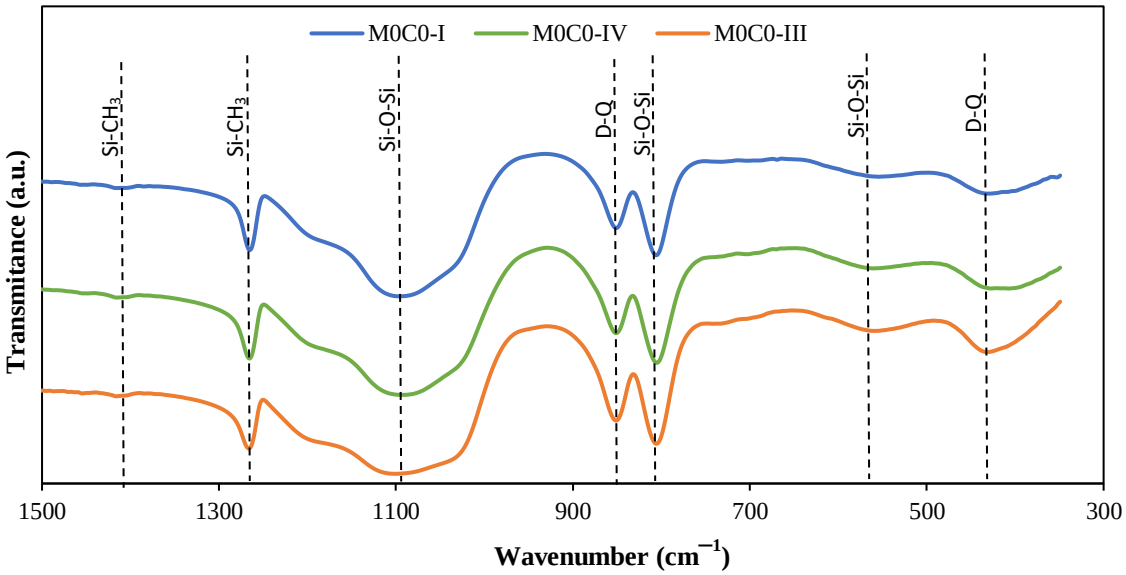

Figure 13. FT-IR spectra of the PDMS-SiO_2 samples in the intervals of: (a) 1500-4000 cm^{-1} (b) 300-1500 cm^{-1}.

1.3. BET analysis

The textural properties of the materials were determined from N^2 adsorption-desorption isotherms using the BET method. The resulting isotherms obtained for the PDMS-SiO_2 samples are presented in Figure 14.

According to the IUPAC classification, the obtained graphics for samples M0C0-I and M0C0-IV are compatible with the type II isotherm, which is usually related to nonporous or macroporous materials, and presents a hysteresis loop (type H3). According to the literature, this type of low pressure hysteresis is caused by the expansion of the non-rigid porous structure of the material, where the final value of the adsorption curve does not coincide with the initial value [160]. The graphic obtained for sample M0C0-III can be associated with the type I isotherm, indicating that the material presents a microporous structure.

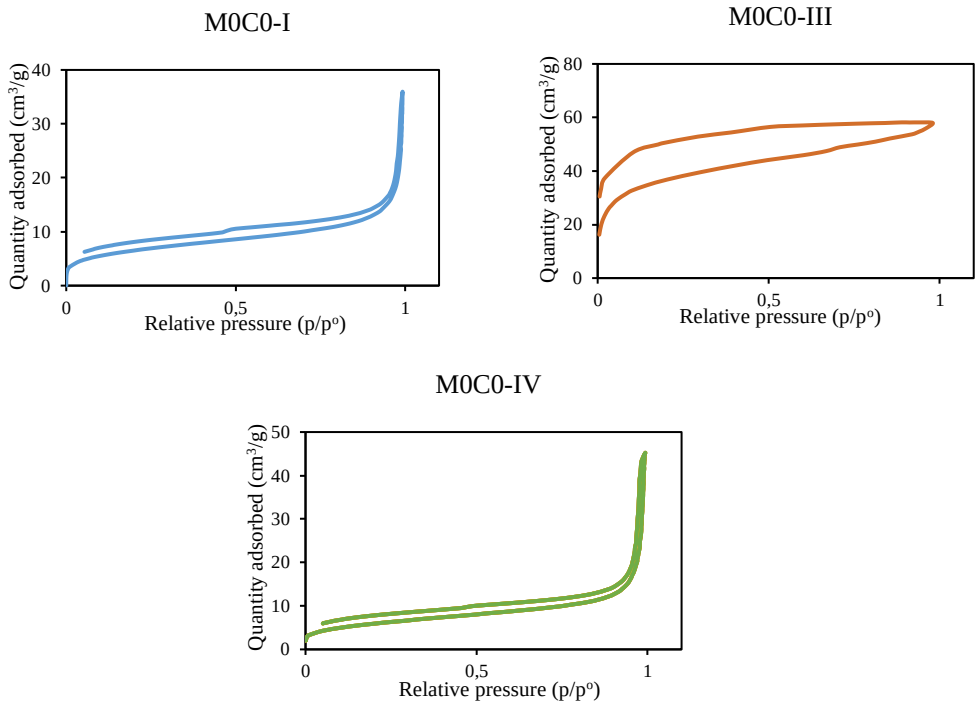

Figure 14. Isotherms of the PDMS-SiO_2 samples obtained by the BET method.

The textural values presented in Table 3 are calculated through the BET adsorption branch of the respective sample and the pore volumes and average diameter were calculated by the BJH (Barrett, Joyner and Halenda) method.

Table 3. Values of surface area calculated from the nitrogen adsorption isotherms, for the PDMS-SiO_2 samples.

	M0C0-I	**M0C0-III**	**M0C0-IV**
BET surface area (m^2 /g)	287.2	122.3	244.9
Pore volume (cm^3/g)	0.990	0.121	0.890
Average pore diameter (nm)	168.9	3.47	99.82

2. Characterization of RES loaded samples

During the loading process, RES molecules can be lodged inside the pores or adsorbed to the surface of the materials. To analyze the RES loaded samples various techniques were used and the results are further explained next.

The X-ray diffractogram of T-RES exhibits multiple diffraction peaks between 5 and 30° which can be attributed to the higher crystallinity of RES when in its "free form". However, when immobilized in the pores of materials, certain substances, such as RES, have a tendency to change the structure of the organic entity from crystalline to amorphous. These results were obtained in a similar system, where RES was encapsulated in MSNs, in which the loading of RES on the nanoparticles promoted the amorphization of the drug[143].

When comparing the T-RES peaks with the diffractograms of the loaded samples, it is clear that the intensity of the peaks (represented in the shaded areas of the graph in Figure 15) drops significantly, indicating RES amorphization after loading. These results showed that, following the loading of the samples, RES had been converted from a crystalline to an amorphous structure, suggesting that it had been successfully incorporated by the material[147,179,180].

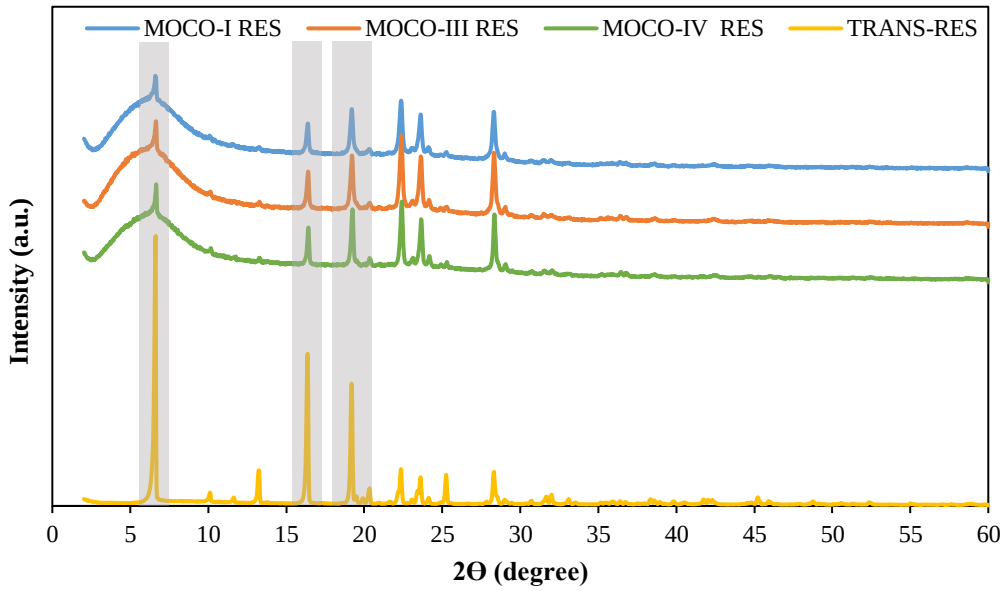

Figure 15. XRD spectra of the PDMS-SiO_2-RES samples and T-RES.

The FT-IR analysis was carried out to evaluate the possible changes that the material might have suffered and determine the bonds established after the loading with RES. Figure 16 presents the FT-IR spectra for each composition obtained before and after RES loading and for free RES. Analyzing the spectra, major changes in the fingerprint region between 400 to 1700 cm^{-1} are clearly noticed when comparing the results of the loaded materials with the unloaded ones, through the appearance of various new bands. The bands situated from around 1600 to 1400 cm^{-1} represent the benzene skeleton vibrations and the ones between 989 and 964 cm^{-1} can be related to bending vibrations of C=C-H[181,182]. The band associated with O-H stretching as shifted from around 3430 to 3280 cm^{-1} in the loaded samples indicating that there is interaction of OH groups of materials with RES. These results are in accordance with the ones previously reported (XRD analysis), and, once again, indicate that RES was successfully loaded into the materials.

(a)

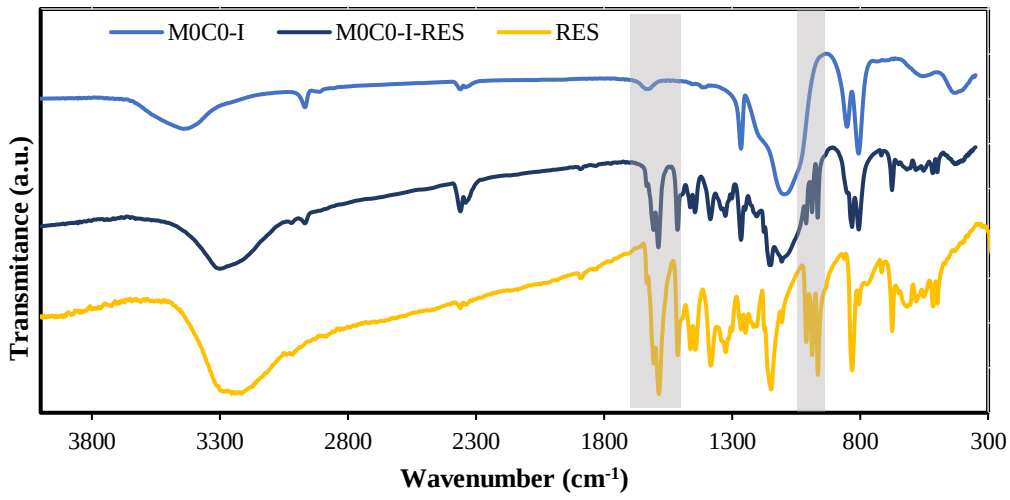

(b)

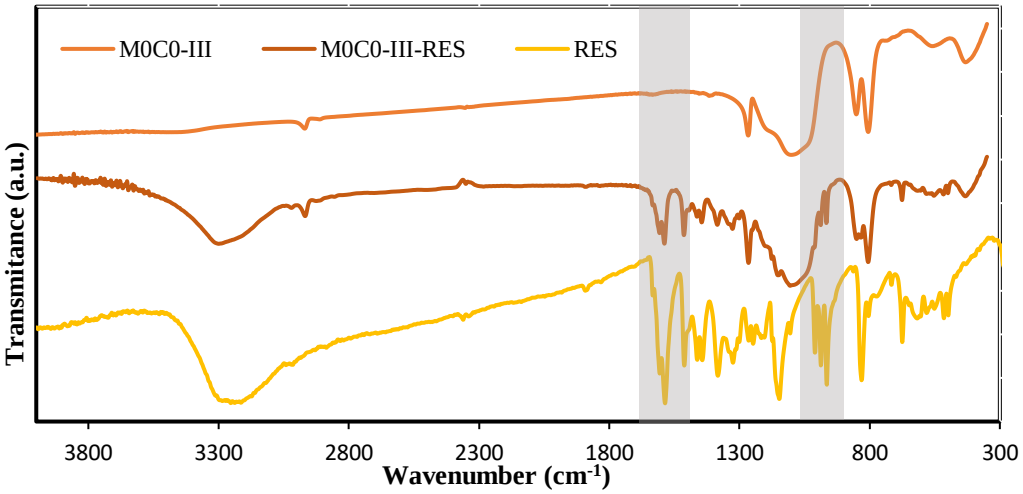

(c)

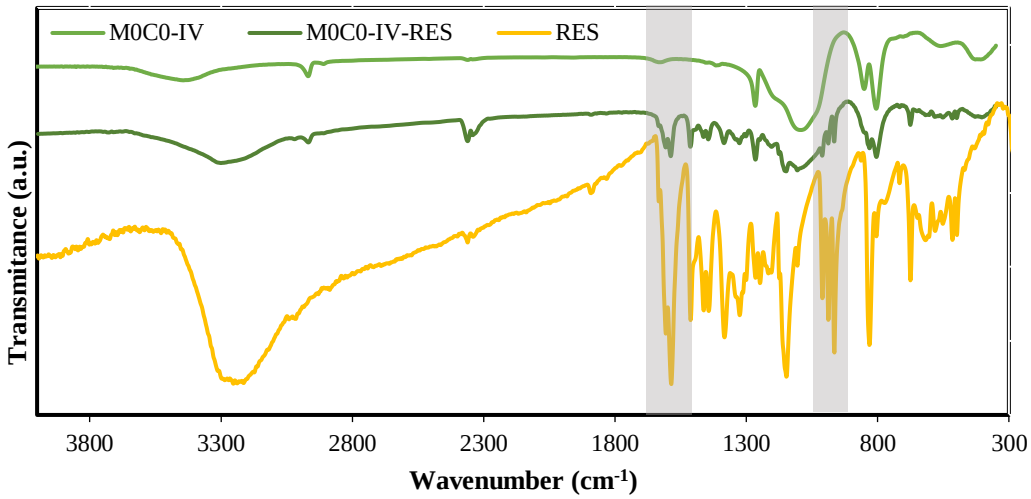

Figure 16. FT-IR spectra of the samples in the interval of 300-4000 cm^{-1}. **(a)** M0C0-I, M0C0-I-RES, and T-RES **(b)** M0C0-III, M0C0-III-RES, and T-RES **(c)** M0C0-IV, M0C0-IV-RES, and T-RES.

The samples (loaded and unloaded) were also analysed by SEM and the obtained images are presented in Figure 17. Observing the images referring to the unloaded materials (M0C0-I, M0C0-III, and M0C0-IV), it is possible to note that these resemble those reported for similar materials present in literature[169]. After the loading of the samples, the presence of aggregates on the surface of the materials, probably RES, is clearly detected, particularly in samples M0C0-I-RES and sample M0C0-IV-RES. In samples without RES in their composition no aggregates were observed in the micrographs.

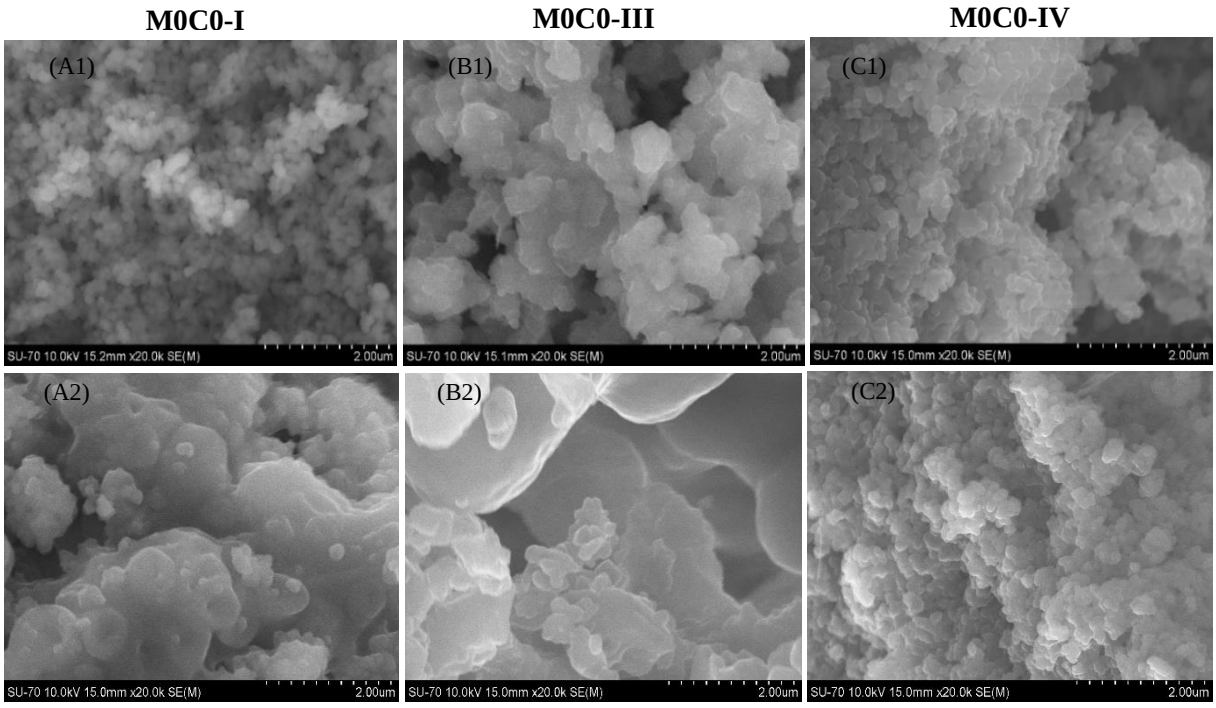

Figure 17. SEM micrographs of the unloaded and loaded samples: (A1) M0C0-I; (A2) M0C0-I-RES; (B1) M0C0-III; (B2) M0C0-III-RES; (C1) M0C0-IV; (C2) M0C0-IV-RES.

2.1 Loading efficiency and capacity

The RES loading capacity and efficiency was evaluated by TGA analysis. Figure 18 presents the curves for both loaded and unloaded materials and free RES. Observing the curves of weight loss (%) versus temperature (ºC) for the unloaded materials it is noticeable that the weight loss of the samples is very small. Around 750ºC all the samples add lost approximately 12% of its initial weight, and the curves almost stabilize for temperatures above 730ºC. This weight loss is caused by the evaporation of adsorbed water molecules present in the samples.

In the case of the RES loaded materials, the weight loss from the samples was much higher, around 51% at 700ºC, with the curves being stable for temperatures above 600ºC. Regarding the curve from RES, it is perceptible that the weight loss occurs in two consecutive phases. A first one, between 240 and 360ºC with a mass loss of 31.8%, which can be associated with the beginning of the thermal decomposition of the material. The second one occurs at approximately 360-550ºC with a weight loss of 66.6% and is attributed

to the oxidation of the carbonized material[183]. A stabilization of the curve is observed for temperatures above 550ºC, and the total weight loss is of 99.3%. The different profiles of the loaded samples curves when compared with the ones from unloaded materials and free RES suggest that the materials have been successfully loaded.

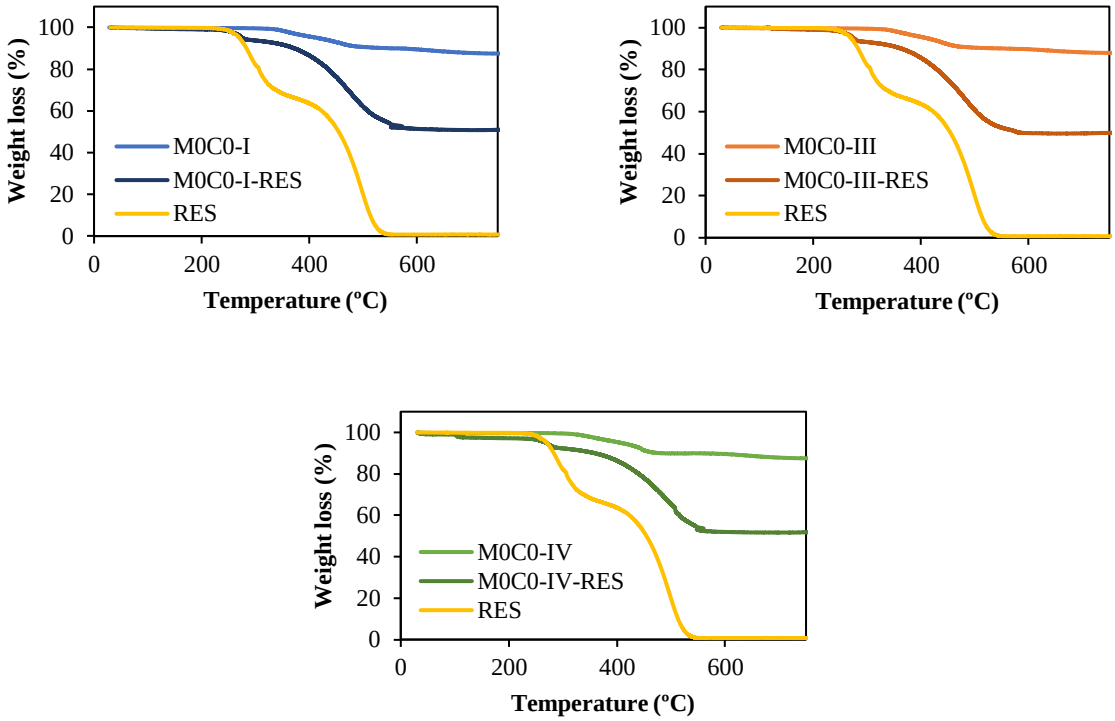

Figure 18. TGA analysis of unloaded and loaded PDMS-SiO_2 samples and pure RES.

The materials were loaded using an initial amount of RES of 160 mg. With the aim of evaluating and calculating the percentage in mass of RES present in the samples, the TGA curves of the RES loaded samples were further analyzed. The results for sample M0C0-I-RES will be explained next and the final results for all the samples are presented in Table 4.

Considering values from 200 to 700 ºC, sample M0C0-I-RES had a weight loss of 48.2%. Since the equivalent unloaded sample had a weight loss of 11,2% in the same temperature interval, it is possible to infer that 36,4% of the weight lost from the loaded sample can be attributed to RES. This value loss corresponds to the loading capacity of the sample. To perform the loading of this sample 160 mg of RES and 200 mg of material were used. If all the RES used had been loaded onto the material, the percentage of RES in the

sample would be 44.4% (theoretical loading capacity). Comparing this value with the loading capacity of the material (Equation 9), we can infer that 82.0% of the RES used was successfully loaded into the material.

$$Loading\ efficiency\ (\%) = \frac{Loading\ capacity}{Theoretical\ loading\ capacity} \cdot 100 \quad \textbf{(9)}$$

Table 4. Values of loading capacity and efficiency for the RES PDMS-SiO_2 loaded samples.

Sample	Loading capacity (%)	Loading efficiency (%)
M0C0-I-RES	36.4	82.0
M0C0-III-RES	37.9	85.4
M0C0-IV-RES	33.7	75.9

2. *In vitro* release studies

3.1. Solubility studies

In order to analyze the solubility of RES in each sample, simple solubility studies were performed. These were set under the same conditions, with a pH of 7.4, that corresponds to the physiological pH. The results observed for each sample and free RES after 24 h are presented in Figure 19.

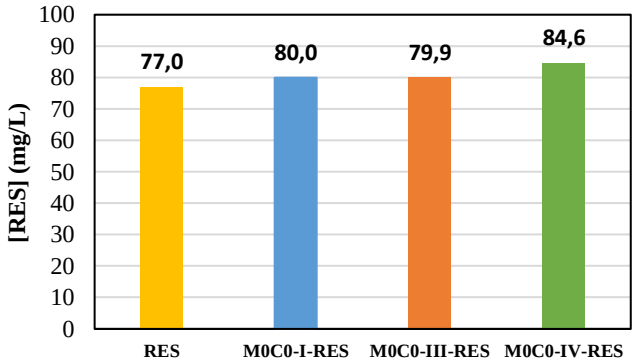

Figure 19. Solubility profiles of the RES loaded samples and pure RES at pH 7.4 after 24 hours.

Observing the results, it is possible to note that all samples presented an increase of the RES concentration when compared to free RES, indicating that these materials can provide a mean to enhance this drug's solubility. When observing these values, it is possible to note that sample M0C0-IV-RES was the one that presented the highest concentration (84.6 mg/L) and, taking into account this result, as well as the characterization analysis performed previously, this was the sample chosen to proceed for the next experiments.

3.2. *In vitro* RES release studies

The cumulative release values of RES from the sample M0C0-IV-RES and free RES (non-encapsulated) at pH 5.2 and 7.4 are presented in Figure 20. Observing the release profiles, the cumulative release values at pH 7.4 after 48 h are 54% and 22% for sample M0C0-IV-RES and RES, respectively, increasing to 70% and 39%, respectively, at pH 5.2. This indicates that the RES release was pH-dependent, being evidently faster in pH 5.2 when compared to pH 7.4, both for sample M0C0-IV-RES and free RES. These results are in agreement with other works found in the literature that studied the stability and solubility of RES in different pH mediums, in which it was found that RES is more stable at acidic conditions, presenting higher values of solubility, and, in contrast, when in alkaline conditions, it is more prone to degradation and, consequentially, presents lower values of solubility. This effect is probably related to the fact that, at higher pH values, the degradation and dissolution mechanisms occur at the same time, resulting in the increase of degraded products and formation of insoluble complexes, thus decreasing RES solubility[184,185].

Additionally, it was also possible to note that the loaded sample was able to reach higher cumulative release values throughout the time at both pH values, when compared to free RES, and demonstrated a gradual and sustained RES release without any initial burst.

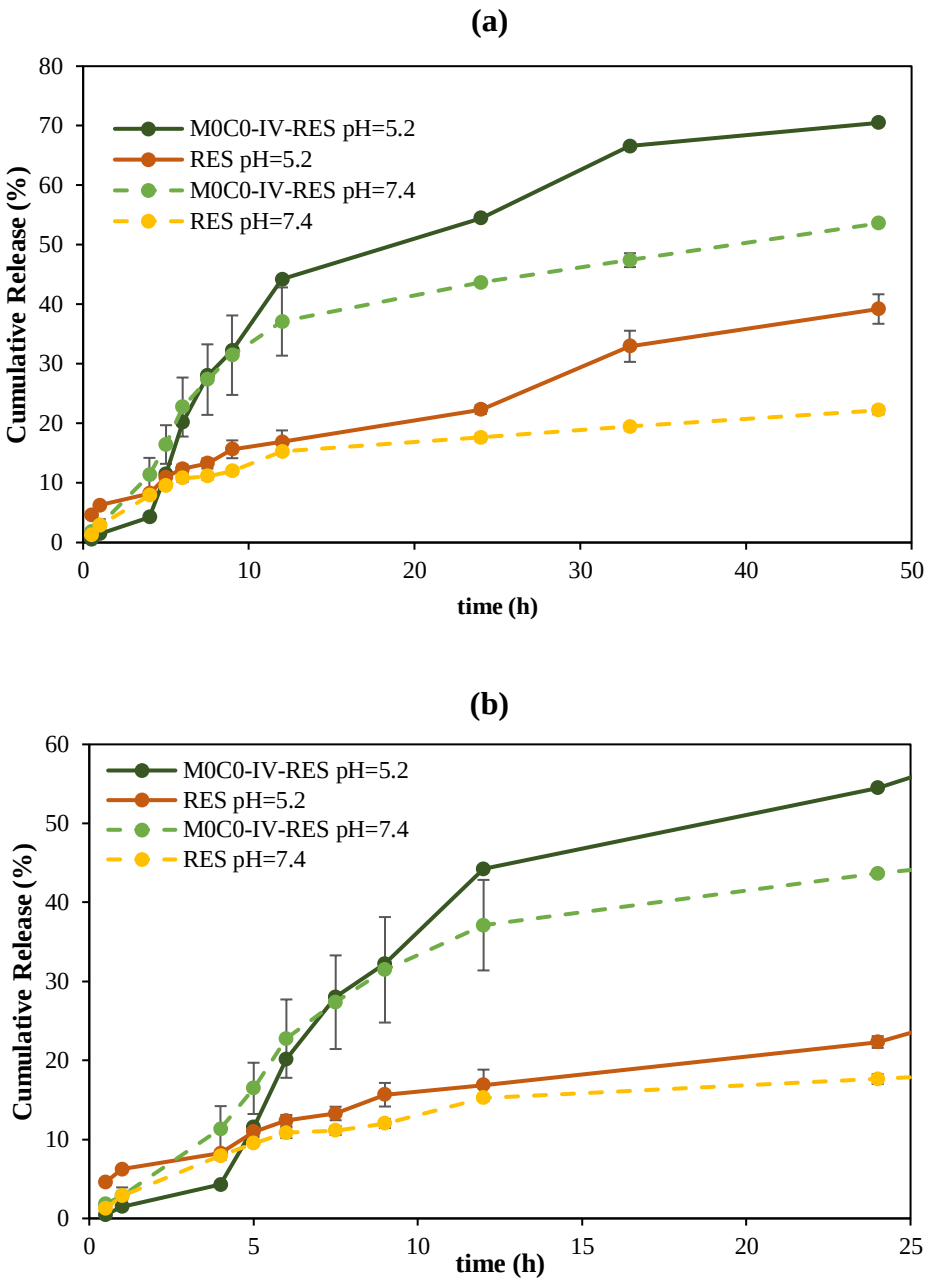

Figure 20. Cumulative release of RES from the non-encapsulated (free RES) and encapsulated sample (M0C0-IV-RES) at pH 5.2 and 7.4. **(a)** Full 48 hours profile; **(b)** First 24 hours profile.

With the purpose of understanding the kinetics and mechanisms of release of RES in the assay, three models were applied to the experimental data: an exponential equation based on the Noyes-Whitney equation applying the Fick's law, the Korsmeyer-Peppas, and the Weibull model. These mathematical models, that combine precise experimental observations with models that capture the underlying physics, have been used to predict the

overall release behaviour of simple and complex DDS, mainly the temporal release of the encapsulated molecule(s)[186].

The first model interprets the drug release data as an exponential type of diffusion based on the Noyes-Whitney equation and the Fick's law (NWF):

$$M_t / M_\infty = 1 - e^{-K_F t} \quad \textbf{(10)}$$

where M_t / M_∞ represents the normalized fraction of the released drug from t=0+ to t=∞, and K_F is the first-order release constant independent of drug concentration, which provides insights on the solvent accessibility to the substrate and the diffusion coefficient through the mesoporous channels[187].

The second model used, Korsmeyer-Peppas (KP) model, is a semi-empirical model based on Fick's second law of diffusion for short time diffusion, which relates the exponential drug release to the elapsed time (t) (Equation (11)):

$$M_t / M_\infty = k_{KP} \cdot t^n \quad \textbf{(11)}$$

where M_t / M_∞ corresponds to the fractional release of the drug, k_{KP} is a constant that incorporates characteristics of the system, and n can be an indicative of the drug release mechanism and can also depend on the geometry of the system. This model is only valid for the portion of the release curve where $M_t / M_\infty < 0.6$[187–189].

Lastly, the final model applied was the Weibull model[187,190,191], an empirical model successfully applied to almost all types of dissolution or release curves, which is described in Equation (12):

$$M_t / M_\infty = 1 - e^{\left(-\frac{(t-Ti)^\beta}{\alpha}\right)} \quad \textbf{(12)}$$

where Mt and M_∞ are the mass of drug released at time t, α defines the time scale of the process, T_i represents the lag time before the onset of the dissolution or release process, and β is the shape parameter that characterizes the curve formed as either: exponential (β=1), S-shaped with upward curve followed by turning point (β > 1), or a curve with higher initial slope and after that consistent with the exponential (β < 1).

From the values of α and β obtained with this model it is also possible to determine the dissolution time, T_d, which represents the time interval necessary to reach 63.2% of drug release (Equation (13)).

$$\alpha = T_d{}^{\beta} \rightarrow T_d = e^{\frac{\log(\alpha)}{\beta}} \quad \textbf{(13)}$$

The curves obtained for each model are presented in Figure 21 and the respective kinetic parameters in Table 5.The experimental data were fitted using non-linear regression by employing the method of least squares and the tool solver of the Origin software, and the goodness of the fitting was evaluated taking into account the values obtained for the statistical parameters of coefficient of determination (R^2) and chi-square (χ^2).

The NWF model didn't present a good fitting in any of the samples analysed, with values of R^2 (ranged from 0,.3 to 0.94) and χ^2 (ranged from 0.003 to 108) far from ideal. For this reason, and because this model didn't accurately describe the release kinetics of the data, the parameters obtained will be disregarded.

From the three models used, the Weibull model was the one that best fitted all the data, presenting higher values of R^2 (between 0.95 and 0.99) and lower values of χ^2 (between 0.0007 and 0.0018). This model was already successfully applied to various drug delivery systems, including for RES release from polymer-based carriers[143,192–194]. In the case of sample M0C0-IV-RES, it was possible to determine a T_i value of 3.9 and 4.6 hours for pH 5.2 and 7.4, respectively, which indicates that the RES release presents a lag time until it reaches a steady release rate. In contrast, for free RES, this value was 0 in both pH analyzed, indicating that this characteristic is intrinsic to the M0C0-IV-RES sample. This may be due to the fact that this sample presents a hydrophobic nature, which may interfere with the release mechanisms and create a delay time for the release of RES. From this model, it was also possible to observe dissolution times, T_d, of 26.75 and 110.31 hours for sample M0C0-IV-RES at pH 5.2 and 7.4, respectively, and 105.01 and 867.49 hours for free RES at the same pH values. These results further confirm that the rate of RES dissolution is pH-dependent for both sample M0C0-IV-RES and RES alone and, that the loaded material improves RES solubility and allows for a faster release rate. Since it is based on an empiric equation, not deducted from any kinetic fundamentals, this model does not provide specifics about the mechanisms of RES release[187].

The KP model was adjusted to the experimental data for a RES cumulative release of up to 0.6 and, presented a good fit for the experimental results obtained for pure RES. However, for sample M0C0-IV-RES, taking into account the values of R^2 (ranged from 0.921 to 0.925) and χ^2 (ranged from 0.0026 to 0.0057), this model was less suitable to describe the experimental data when compared to the Weibull model. The values of k_{KP} obtained for sample M0C0-IV-RES were 0.07 and 0.09 at pH 5.2 and 7.4, respectively, and 0.043 and 0.047 for free RES at the same pH values. These values are an indicator of the characteristics of the system, which means that for free RES, the change in the medium pH may have changed the system characteristics, in the case of sample M0C0-IV-RES, since it is loaded with RES, the observed increase can possibly be attributed to the changes in the RES present in the loaded material, which, consequently, changes the characteristics of the whole system. For both sample M0C0-IV-RES and free RES at the two pH values analysed, the values of *n* range from 0.41 to 0.68, which can be related to a non-Fickian model of transport[187,188].

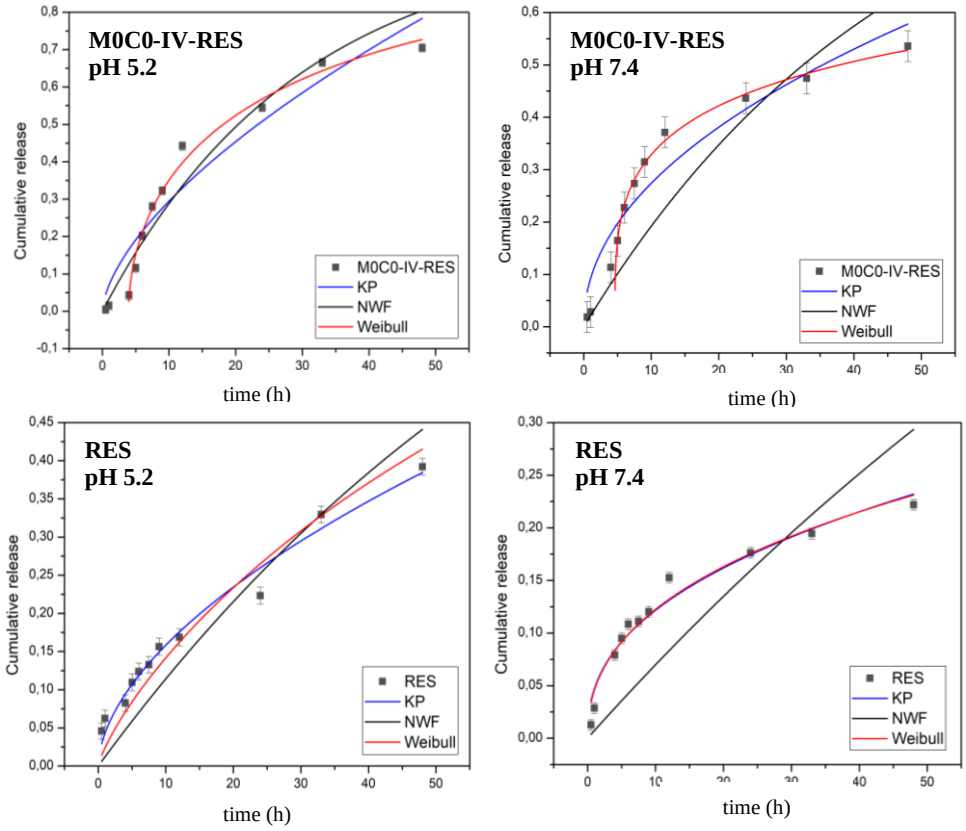

Figure 21. Fitting of each model (KP, NWF and Weibull) for sample M0C0-IV-RES and free RES at pH 5.2 and 7.4.

Table 5. Kinetic parameters and goodness of the fits of RES release from sample M0C0-IV-RES and pure RES.

Model		M0C0-IV-RES		RES	
		pH 5.2	pH 7.4	pH 5.2	pH 7.4
Korsmeyer-Peppas	k_{KP} (h^{-1})	0.07 ± 0.02	0.09 ± 0.02	0.043 ± 0.005	0.047 ± 0.005
	n	0.62 ± 0.08	0.48 ± 0.06	0.57 ± 0.03	0.41 ± 0.03
	R^2	0.9218	0.9257	0.9777	0.9625
	χ^2	0.0057	0.0026	0.0003	0.0002
Weibull	α (h^{β})	6.3 ± 0.6	4.1 ± 0.9	41.4 ± 0.1	21 ± 2
	β	0.56 ± 0.03	0.30 ± 0.07	0.80 ± 0.01	0.45 ± 0.03
	T_i (h)	3.93 ± 0.09	4.6 ± 0.5	0	0
	T_d (h)	26.75	110.31	105.01	867.49
	R^2	0.9919	0.9533	0.9782	0.9670
	χ^2	0.0007	0.0018	0.0003	0.0002

4. Cell viability studies

The cytotoxicity of sample M0C-IV-RES, free RES (non-encapsulated) and pristine M0C0-IV on MG-63 osteosarcoma cells was evaluated using the MTT cell viability assay, and the results obtained are shown in Figure 22.

Observing Figure 22 (a), it is possible to note that cell viability remained unchanged in the case of the M0C0-IV sample independently of the concentration used, with values ranging between 94% and 98% compared to the control. This result is in agreement with previous studies, in which it was possible to observe that similar silica-based materials did not cause cytotoxicity in this type of cells[195,196].

For sample M0C0-IV-RES (Figure 22 (b)), a gradual decrease in cell viability is noticeable with increasing concentration of the sample used (for concentrations > 100 µg mL^{-1}), with a percentage of cell viability of 18.1% for the highest concentration of sample studied (350 µg mL^{-1}). However, when comparing these results with the ones from non-loaded RES (Figure 22 (c)), similar RES concentrations (in the loaded sample and bulk RES) give rise to very different percentages of cell viability. In the case of the highest concentration of bulk RES studied (500 µM) a percentage of cell viability of 63.3% was

obtained, while for a similar concentration of RES present in the loaded sample (518 µM) this value was 18.1%, and this trend is repeated for all RES concentrations higher than 150µM studied. These results indicate that, for an equal time interval, there was a greater release of RES from the M0C0-IV-RES sample, consequently having a greater effect on cell viability when compared to RES alone, and further confirming the previous results obtained in the release studies.

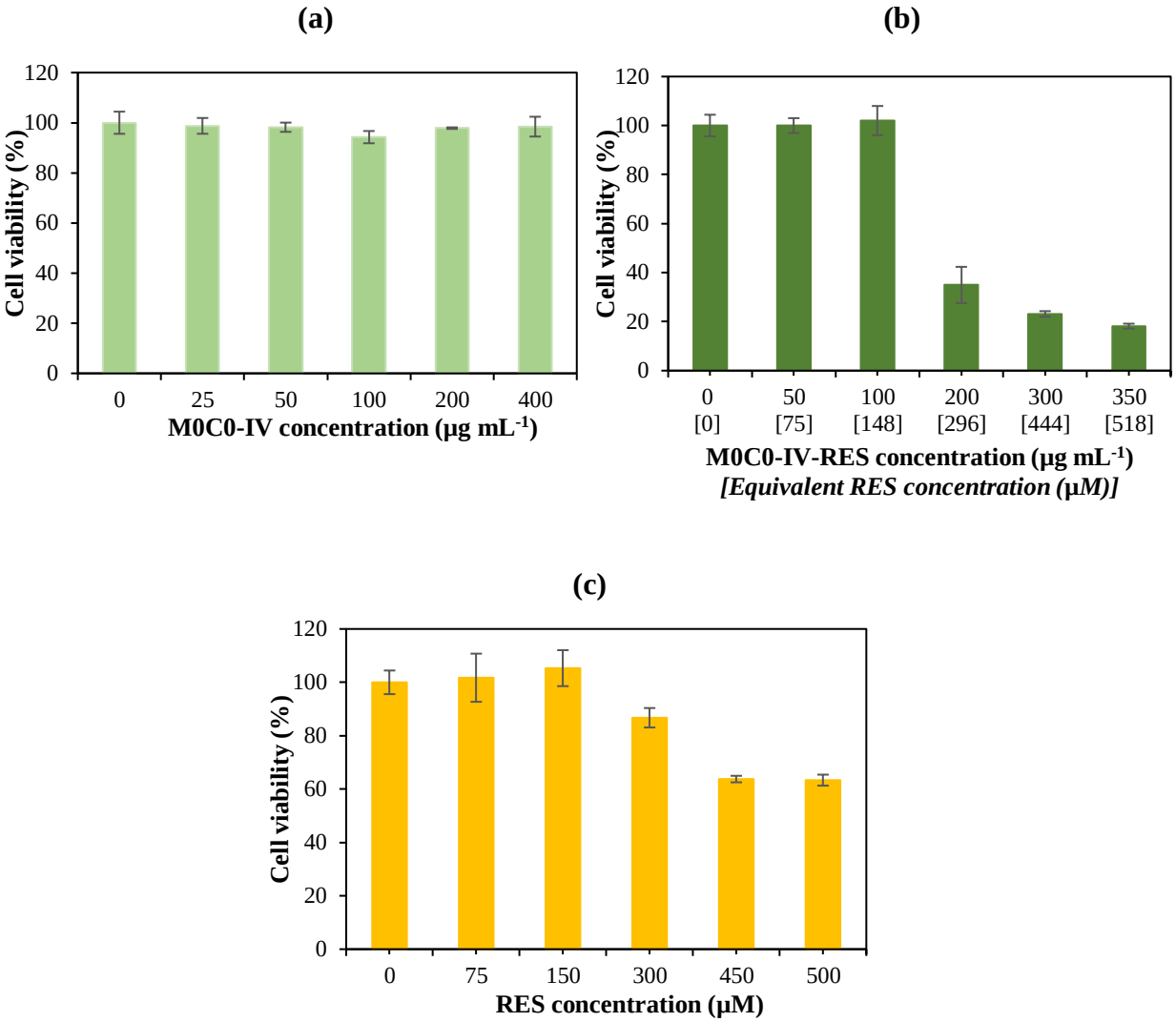

Figure 22. Effect of pristine M0C0-IV (0-400 µg/mL; **(a)**) , RES-loaded M0C0-IV (0–350 µg/mL, **(b)**), and bulk RES (0–500 µM, **(c)**) on cell viability of MG-63 osteosarcoma cells after 24h of exposure.

V. Conclusions and future perspectives

Various disorders/defects, such as osteoporosis or osteosarcoma, can lead to bone tissue damage and consequent bone loss. The bone grafting techniques used present several limitations, highlighting the need for synthetic materials capable of replacing the ones presently used. The constant development in the field of biomaterials - already capable of offering options that mimic biological conditions in an unprecedented way - opens the door to regenerative medical approaches that could be considered the future in treatment options to enhance bone healing. ORMOSILs - organic-inorganic hybrid materials obtained through the sol-gel method - showed their great potential in the field of bone tissue engineering with several biomedical applications from an early age.

In this work, the PDMS-SiO_2 system was explored, using the specific properties of its organic and inorganic components in order to create a network with interactions between the components resulting in a material with tunable morphology, size, and multifunctional properties. Four types of materials were synthesized (M0C0-I, M0C0-II, M0C0-III, and M0C0-IV), using different concentrations of H_2O and HCl, and subsequently characterized using various techniques: X-Ray Diffraction (XRD), Fourier Transform Infrared (FTIR) spectroscopy, specific surface area by the Brumauer-Emmet-Teller (BET), Scanning Electron Microscopy (SEM) and Thermogravimetric Analysis (TGA). The incorporation of RES into the hybrid materials was successfully performed using the rotary evaporation technique, allowing to achieve loading capacities ranging from 75.9% to 85.4%.

After the characterization of the loaded samples, it was possible to perceive that the loading promoted the amorphization of RES, increasing its solubility. This was confirmed by the release assays performed (only carried out for sample M0C0-IV-RES), in which it was quite noticeable that the RES release was much more pronounced in the case of sample M0C0-IV-RES compared to RES alone. It was also determined that the release of RES is pH-dependent, having been obtained percentages of release after 48 hours of 70% and 54% for sample M0C0-IV-RES at pH 5.2 and 7.4, respectively, and of 39% and 22% in the case of free RES at the same pH values.

Through the mathematical analysis performed on the data (using the NWF model, the Weibull model and the KP model), it was noticeable that the model that best fitted the

experimental data was the Weibull model. This analysis allowed to obtain important data regarding the RES release kinetics. In the case of sample M0C0-IV-RES, it was possible to determine an initial time lag of approximately 4 hours, regardless of the pH used, something that was not observed with free RES.

The cytotoxicity of the material was analysed by an MTT cell viability assay on osteosarcoma MG-63 cells. Sample M0C0-IV (unloaded) showed no cytotoxicity to cells, regardless of the concentration being used. In the case of the loaded sample, a gradual decrease in cell viability was observed for concentrations above 100 μg mL^{-1}. Comparing the values obtained for the loaded sample and the bulk RES, it is notable that, for the same concentrations of RES, different values of cell viability were obtained, which, in the case of the loaded sample, were much lower. This indicates that, when incorporated in the sample, RES has a higher release rate and, consequently, a greater effect on cells.

In summary, the results of our research indicate that these materials, which combine the physicochemical properties of the PDMS-SiO_2 system with the biological properties of RES, present enormous potential to be used in the fields of synthetic bone grafts and DDS for RES.

Although the objectives of this work have been successfully achieved, there are still aspects that could be further explored. Moving forward, it would be interesting to synthetize the hybrid materials incorporating important ions, such as calcium or strontium, in order to improve the materials biological properties. Regarding the characterization of the materials, more analysis could be performed to better understand the molecular accommodation and the nature of the bonds formed between RES and the hybrid materials. Also, concerning the RES loading technique used, other approaches could be studied, such as the incorporation of RES at the beginning of the synthesis of the materials and the incorporation of RES in other forms of the material (monolith, film).

Another important step is testing the effectiveness of the materials to serve as DDS for other compounds with interesting and relevant pharmacological activities.

References

1. Iaquinta, M. R., Mazzoni, E., Manfrini, M., D'Agostino, A., Trevisiol, L., Nocini, R., Trombelli, L., Barbanti-Brodano, G., Martini, F. and Tognon, M. Innovative biomaterials for bone regrowth. *Int J Mol Sci* **20**, 1–17 (2019).

2. Tu, K. N., Lie, J. D., Wan, C. K. V., Cameron, M., Austel, A. G., Nguyen, J. K., Van, K. and Hyun, D. Osteoporosis: A review of treatment options. *P and T* **43**, 92–104 (2018).

3. Onishi, K., Utturkar, A., Chang, E., Panush, R., Hata, J. and Perret-Karimi, D. Osteoarthritis: A Critical Review. *Crit Rev Phys Rehabil Med* **24**, 251–264 (2012).

4. Cortini, M., Baldini, N. and Avnet, S. New advances in the study of bone tumors: A lesson from the 3D environment. *Front Physiol* **10**, 1–8 (2019).

5. Svedbom, A., Hernlund, E., Ivergård, M., Compston, J., Cooper, C., Stenmark, J., McCloskey, E. v., Jönsson, B. and Kanis, J. A. Osteoporosis in the European Union: A compendium of country-specific reports. *Arch Osteoporos* **8**, (2013).

6. Kanis, J. A., Norton, N., Harvey, N. C., Jacobson, T., Johansson, H., Lorentzon, M., McCloskey, E. v., Willers, C. and Borgström, F. SCOPE 2021: a new scorecard for osteoporosis in Europe. *Arch Osteoporos* **16**, (2021).

7. Stiller, C. A., Botta, L., Brewster, D. H., Ho, V. K. Y., Frezza, A. M., Whelan, J., Casali, P. G., Trama, A. and Gatta, G. Survival of adults with cancers of bone or soft tissue in Europe: Report from the EUROCARE-5 study. *Cancer Epidemiol* **56**, 146–153 (2018).

8. Aslankoohi, N., Mondal, D., Rizkalla, A. S. and Mequanint, K. Bone repair and regenerative biomaterials: Towards recapitulating the microenvironment. *Polymers (Basel)* **11**, (2019).

9. Wang, W. and Yeung, K. W. K. Bone grafts and biomaterials substitutes for bone defect repair: A review. *Bioact Mater* **2**, 224–247 (2017).

10. Schemitsch, E. H. Size Matters: Defining Critical in Bone Defect Size! *J Orthop Trauma* **31**, S20–S22 (2017).

11. Baldwin, P., Li, D. J., Auston, D. A., Mir, H. S., Yoon, R. S. and Koval, K. J. Autograft, Allograft, and Bone Graft Substitutes: Clinical Evidence and Indications for Use in the Setting of Orthopaedic Trauma Surgery. *J Orthop Trauma* **33**, 203–213 (2019).

12. Ates, B., Koytepe, S., Balcioglu, S., Ulu, A. and Gurses, C. Biomedical applications of hybrid polymer composite materials. *Hybrid Polymer Composite Materials: Applications* 343–408 (2017).

13. Tang, G., Liu, Z., Liu, Y., Yu, J., Wang, X., Tan, Z. and Ye, X. Recent Trends in the Development of Bone Regenerative Biomaterials. *Front Cell Dev Biol* **9**, 1–18 (2021).

14. Wen, J. and Wilkes, G. L. Organic/inorganic hybrid network materials by the sol-gel approach. *Chemistry of Materials* **8**, 1667–1681 (1996).

15. Jones, J. R. Review of bioactive glass: From Hench to hybrids. *Acta Biomater* **23**, 53–82 (2015).

16. Valliant, E. M. and Jones, J. R. Softening bioactive glass for bone regeneration: Sol-gel hybrid materials. *Soft Matter* **7**, 5083–5095 (2011).

17. Mizokami, A., Kawakubo-Yasukochi, T. and Hirata, M. Osteocalcin and its endocrine functions. *Biochem Pharmacol* **132**, 1–8 (2017).

18. Riddle, R. C. and Clemens, T. L. Bone cell bioenergetics and skeletal energy homeostasis. *Physiol Rev* **97**, 667–698 (2017).

19. Han, Y., You, X., Xing, W., Zhang, Z. and Zou, W. Paracrine and endocrine actions of bone - The functions of secretory proteins from osteoblasts, osteocytes, and osteoclasts. *Bone Res* **6**, 1–11 (2018).

20. Lopes, D., Martins-Cruz, C., Oliveira, M. B. and Mano, J. F. Bone physiology as inspiration for tissue regenerative therapies. *Biomaterials* **185**, 240–275 (2018).

21. Clarke, B. Normal bone anatomy and physiology. *Clinical journal of the American Society of Nephrology* **3**, (2008).

22. Lafon, J. P., Champion, E. and Bernache-Assollant, D. Processing of AB-type carbonated hydroxyapatite Ca10-x(PO4)6-x(CO3)x(OH)2-x-2y(CO3)y ceramics with controlled composition. *J Eur Ceram Soc* **28**, 139–147 (2008).

23. Henkel, J., Woodruff, M. A., Epari, D. R., Steck, R., Glatt, V., DIckinson, I. C., Choong, P. F. M., Schuetz, M. A. and Hutmacher, Di. W. Bone Regeneration Based on Tissue Engineering Conceptions: A 21st Century Perspective. *Bone Res* **1**, 216–248 (2013).

24. Bhattarai, D. P., Aguilar, L. E., Park, C. H. and Kim, C. S. A review on properties of natural and synthetic based electrospun fibrous materials for bone tissue engineering. *Membranes (Basel)* **8**, (2018).

25. Sanchez, C., Julián, B., Belleville, P. and Popall, M. Applications of hybrid organic-inorganic nanocomposites. *J Mater Chem* **15**, 3559–3592 (2005).

26. Raghavendra, G. M., Varaprasad, K. and Jayaramudu, T. Biomaterials: Design, Development and Biomedical Applications. *Nanotechnology Applications for Tissue Engineering* 21–44 (2015).

27. Williams, D. F. On the mechanisms of biocompatibility. *Biomaterials* **29**, 2941–2953 (2008).

28. Albrektsson, T. and Johansson, C. Osteoinduction, osteoconduction and osseointegration. *European Spine Journal* **10**, S96–S101 (2001).

29. Parithimarkalaignan, S. and Padmanabhan, T. v. Osseointegration: An update. *Journal of Indian Prosthodontist Society* **13**, 2–6 (2013).

30. Qu, H., Fu, H., Han, Z. and Sun, Y. Biomaterials for bone tissue engineering scaffolds: A review. *RSC Adv* **9**, 26252–26262 (2019).

31. Ratner, B. D. Biomaterials: Been There, Done That, and Evolving into the Future. *Annu Rev Biomed Eng* **21**, 171–191 (2019).

32. Valliant, E. M. and Jones, J. R. Softening bioactive glass for bone regeneration: sol-gel hybrid materials. *Soft Matter* **7**, 5083–5095 (2011).

33. Haugen, H. J., Lyngstadaas, S. P., Rossi, F. and Perale, G. Bone grafts: which is the ideal biomaterial? *J Clin Periodontol* **46**, 92–102 (2019).

34. Ducheyne, P. and Qiu, Q. Bioactive ceramics: The effect of surface reactivity on bone formation and bone cell function. *Biomaterials* **20**, 2287–2303 (1999).

35. Das, P. P., Chaudhary, V., Kumar Singh, R., Singh, D. and Aditya Bachchan, A. Advancement in hybrid materials, its applications and future challenges: A review. *Mater Today Proc* **47**, 3794–3801 (2021).

36. Singh, A., Verma, N. and Kumar, K. Hybrid composites: A revolutionary trend in biomedical engineering. *lMaterials for Biomedica Engineering: Bioactive Materials, Properties, and Applications* 33–46 (2019).

37. Fahmi, A., Pietsch, T., Mendoza, C. and Cheval, N. Functional hybrid materials. *Materials Today* **12**, 44–50 (2009).

38. Soares, P. I. P., Echeverria, C., Baptista, A. C., João, C. F. C., Fernandes, S. N., Almeida, A. P. C., Silva, J. C., Godinho, M. H. and Borges, J. P. Hybrid polysaccharide-based systems for biomedical applications. *Hybrid Polymer Composite Materials: Applications* 107–149 (2017).

39. Wegst, U. G. K., Bai, H., Saiz, E., Tomsia, A. P. and Ritchie, R. O. Bioinspired structural materials. *Nat Mater* **14**, 23–36 (2015).

40. Graham, T. On the properties of silicic acid and other analogous substances. *J Chem Soc* **17**, 318–327 (1864).

41. Owens, G. J., Singh, R. K., Foroutan, F., Alqaysi, M., Han, C. M., Mahapatra, C., Kim, H. W. and Knowles, J. C. Sol-gel based materials for biomedical applications. *Prog Mater Sci* **77**, 1–79 (2016).

42. Hench, L. L. and West, J. K. The sol-gel process. *Chem Rev* **90**, 33–72 (1990).

43. Sousa, R. P. C. L., Ferreira, B., Azenha, M., Costa, S. P. G., Silva, C. J. R. and Figueira, R. B. PDMS based hybrid sol-gel materials for sensing applications in alkaline environments: Synthesis and characterization. *Polymers (Basel)* **12**, (2020).

44. C.J. Brinker; G. W. Scherer. Sol-Gel Science: The physics and chemistry of sol-gel processing. (1990).

45. Philipp, G. and Schmidt, H. New materials for contact lenses prepared from Si- and Ti-alkoxides by the sol-gel process. *J Non Cryst Solids* **63**, 283–292 (1984).

46. Feinle, A., Elsaesser, M. S. and Hüsing, N. Sol-gel synthesis of monolithic materials with hierarchical porosity. *Chem Soc Rev* **45**, 3377–3399 (2016).

47. Danks, A. E., Hall, S. R. and Schnepp, Z. The evolution of 'sol-gel' chemistry as a technique for materials synthesis. *Mater Horiz* **3**, 91–112 (2016).

48. Meinusch, R., Ellinghaus, R., Hormann, K., Tallarek, U. and Smarsly, B. M. On the underestimated impact of the gelation temperature on macro- and mesoporosity in monolithic silica. *Physical Chemistry Chemical Physics* **19**, 14821–14834 (2017).

49. Yang, P., Gai, S. and Lin, J. Functionalized mesoporous silica materials for controlled drug delivery. *Chem Soc Rev* **41**, 3679–3698 (2012).

50. Mackenzie, J. D. and Bescher, E. P. Structures, Properties and Potential Applications of Ormosils. *J Solgel Sci Technol* **31**, 371–377 (1998).

51. Tathe, A., Ghodke, M. and Nikalje, A. P. A brief review: Biomaterials and their apllication. *Int J Pharm Pharm Sci* **2**, 19–23 (2010).

52. Merve, A. , V. W. Y. Hybrid Materials: Historical perspective and current trends. *Eurofillers Polymerblends* 1–23 (2020).

53. Kickelbick, G. Hybrid Materials – Past, Present and Future. *Hybrid Materials* **1**, (2014).

54. Malucelli, G. Hybrid organic/inorganic coatings through dual-cure processes: State of the art and perspectives. *Coatings* **6**, (2016).

55. Criado, M., Sobrados, I. and Sanz, J. Polysiloxane hybrids via sol-gel process: Effect of temperature on network formation. *Coatings* **10**, 1–14 (2020).

56. Huang, H.-H., Orler, B. and Wilkes, G. L. Ceramers: Hybrid materials incorporating polymeric/oligomeric species with inorganic glasses by a sol-gel process. *Polymer Bulletin* **16**, 94–94 (1985).

57. Sur, G. S. and Mark, J. E. Elastomeric networks cross-linked by silica or titania fillers. *Eur Polym J* **21**, 1051–1052 (1985).

58. Ren, L. F., Liu, C., Xu, Y., Zhang, X., Shao, J. and He, Y. High-performance electrospinning-phase inversion composite PDMS membrane for extractive membrane bioreactor: Fabrication, characterization, optimization and application. *J Memb Sci* **597**, 117624 (2020).

59. Giri, R., Naskar, K. and Nando, G. B. Effect of electron beam irradiation on dynamic mechanical, thermal and morphological properties of LLDPE and PDMS rubber blends. *Radiation Physics and Chemistry* **81**, 1930–1942 (2012).

60. Montazerian, H., Mohamed, M. G. A., Montazeri, M. M., Kheiri, S., Milani, A. S., Kim, K. and Hoorfar, M. Permeability and mechanical properties of gradient porous PDMS scaffolds fabricated by 3D-printed sacrificial templates designed with minimal surfaces. *Acta Biomater* **96**, 149–160 (2019).

61. Rao, H., Zhang, Z. and Liu, F. Enhanced mechanical properties and blood compatibility of PDMS/liquid crystal cross-linked membrane materials. *J Mech Behav Biomed Mater* **20**, 347–353 (2013).

62. Wolf, M. P., Salieb-Beugelaar, G. B. and Hunziker, P. PDMS with designer functionalities—Properties, modifications strategies, and applications. *Prog Polym Sci* **83**, 97–134 (2018).

63. Ariati, R., Sales, F., Souza, A., Lima, R. A. and Ribeiro, J. Polydimethylsiloxane Composites Characterization and Its Applications: A Review. *Polymers (Basel)* **13**, 4258 (2021).

64. Serban, B. A., Barrett-Catton, E. and Serban, M. A. Tetraethyl orthosilicate-based hydrogels for drug delivery—effects of their nanoparticulate structure on release properties. *Gels* **6**, 1–10 (2020).

65. Babonneau, F., Thorne, K. and Mackenzie, J. D. Dimethyldiethoxysilane/tetraethoxysilane copolymers: precursors for the silicon-carbon-oxygen system. *Chemistry of Materials* **1**, 554–558 (1989).

66. Salinas, A. J., Merino, J. M., Babonneau, F. and Gil, F. J. Microstructure and Macroscopic Properties of BioactiveCaO–SiO2–PDMS Hybrids. *Wiley Periodical* **81 B**, 274–282 (2006).

67. Brinker, C. J. Hydrolysis and Condensation of Silicates: Effects on Structure. *J Non Cryst Solids* **100**, 31–50 (1988).

68. Coradin, T., Boissiere, M. and Livage, J. Sol-gel Chemistry in Medicinal Science. *Curr Med Chem* **13**, 99–108 (2009).

69. Cypryk, M. and Apeloig, Y. Mechanism of the acid-catalyzed Si-O bond cleavage in siloxanes and siloxanols. A theoretical study. *Organometallics* **21**, 2165–2175 (2002).

70. Iwamoto, T., Morita, K. and Mackenzie, J. D. Liquid-State Si-29 Nmr-Study on the Sol-Gel Reaction-Mechanisms of Ormosils. *J Non Cryst Solids* **159**, 65–72 (1993).

71. Hu, Y. and Mackenzie, J. D. Rubber-like elasticity of organically modified silicates. *J Mater Sci* **27**, 4415–4420 (1992).

72. Coan, T., Barroso, G. S., MacHado, R. A. F., de Souza, F. S., Spinelli, A. and Motz, G. A novel organic-inorganic PMMA/polysilazane hybrid polymer for corrosion protection. *Prog Org Coat* **89**, 220–230 (2015).

73. Tiwari, I. and Mahanwar, P. A. Polyacrylate/silica hybrid materials: A step towards multifunctional properties. *J Dispers Sci Technol* **40**, 925–957 (2019).

74. Kargozar, S., Baino, F., Hamzehlou, S., Hill, R. G. and Mozafari, M. Bioactive glasses entering the mainstream. *Drug Discov Today* **23**, 1700–1704 (2018).

75. Lu, X., Li, K., Xie, Y., Qi, S., Shen, Q., Yu, J., Huang, L. and Zheng, X. Improved osteogenesis of boron incorporated calcium silicate coatings via immunomodulatory effects. *J Biomed Mater Res A* **107**, 12–24 (2019).

76. Glenske, K., Donkiewicz, P., Köwitsch, A., Milosevic-Oljaca, N., Rider, P., Rofall, S., Franke, J., Jung, O., Smeets, R., Schnettler, R., Wenisch, S. and Barbeck, M. Applications of metals for bone regeneration. *Int J Mol Sci* **19**, (2018).

77. Tsuru, K., Aburatani, Y., Yabuta, T., Hayakawa, S., Ohtsuki, C. and Osaka, A. Synthesis and In Vitro Behavior of Organically Modified Silicate Containing Ca Ions. *J Solgel Sci Technol* **21**, 89–96 (2001).

78. Tavares, M. T., Oliveira, M. B., Mano, J. F., Farinha, J. P. S. and Baleizão, C. Bioactive silica nanoparticles with calcium and phosphate for single dose osteogenic differentiation. *Materials Science and Engineering C* **107**, (2020).

79. Zeng, J., Guo, J., Sun, Z., Deng, F., Ning, C. and Xie, Y. Osteoblastic and anti-osteoclastic activities of strontium-substituted silicocarnotite ceramics: In vitro and in vivo studies. *Bioact Mater* **5**, 435–446 (2020).

80. Aimaiti, A., Maimaitiyiming, A., Boyong, X., Aji, K., Li, C. and Cui, L. Low-dose strontium stimulates osteogenesis but high-dose doses cause apoptosis in human adipose-derived stem cells via regulation of the ERK1/2 signaling pathway. *Stem Cell Res Ther* **8**, (2017).

81. Marie, P. J. Strontium ranelate: New insights into its dual mode of action. *Bone* **40**, (2007).

82. Salehi, B., Mishra, A. P., Nigam, M., Sener, B., Kilic, M., Sharifi-Rad, M., Fokou, P. V. T., Martins, N. and Sharifi-Rad, J. Resveratrol: A double-edged sword in health benefits. *Biomedicines* **6**, 1–20 (2018).

83. Akinwumi, B. C., Bordun, K. A. M. and Anderson, H. D. Biological activities of stilbenoids. *Int J Mol Sci* **19**, 1–25 (2018).

84. Anisimova, N. Y., Kiselevsky, M. v, Sosnov, A. v, Sadovnikov, S. v, And, I. N. S. and Gakh, A. A. Trans-, cis-, and dihydro-resveratrol: a comparative study. *Chem Cent J* **5**, (2011).

85. Montsko, G., Nikfardjam, M. S. P., Szabo, Z., Boddi, K., Lorand, T., Ohmacht, R. and Mark, L. Determination of products derived from trans-resveratrol UV photoisomerisation by means of HPLC-APCI-MS. *J Photochem Photobiol A Chem* **196**, 44–50 (2008).

86. Blache, D., Rustan, I., Durand, P., Lesgards, G. and Loreau, N. Gas chromatographic analysis of resveratrol in plasma, lipoproteins and cells after in vitro incubations. *Journal of Chromatography B* **702**, 103–110 (1997).

87. Baslyt, J.-P., Marre-Fournier, F., le Bail, J.-C., Habrioux, G. and Chulia, A. J. Estrogenic/Antiestrogenic and Scavenging Properties of (E)- and (Z)-Resveratrol. *Life Sci* **66**, 769–777 (2000).

88. Siemann, E. H. and Creasy, L. L. Concentration of the Phytoalexin Resveratrol in Wine. *Am J Enol Vitic* **43**, (1992).

89. Renaud, S. and Lorgeril, M. de. Wine, alcohol, platelets, and the French paradox for coronary heart disease. *The Lancet* **339**, 1523–1526 (1992).

90. Koushki, M., Amiri-Dashatan, N., Ahmadi, N., Abbaszadeh, H. A. and Rezaei-Tavirani, M. Resveratrol: A miraculous natural compound for diseases treatment. *Food Sci Nutr* **6**, 2473–2490 (2018).

91. Fiod Riccio, B. V., Fonseca-Santos, B., Colerato Ferrari, P. and Chorilli, M. Characteristics, Biological Properties and Analytical Methods of Trans-Resveratrol. *Crit Rev Anal Chem* **50**, 339–358 (2020).

92. Cheol Ryong Ku, Hyeon Jeong Lee, Suk Kyoung Kim, Eun Young Lee, Mi-Kyung Lee and Eun Jig Lee. Resveratrol prevents streptozotocin-induced diabetes by inhibiting the apoptosis of pancreatic β-cell and the cleavage of poly (ADP-ribose) polymerase. *Endocr J* **59**, 103–109 (2012).

93. M. Thadhani, V. Resveratrol in Management of Diabetes and Obesity: Clinical Applications, Bioavailability, and Nanotherapy. *Resveratrol - Adding Life to Years, Not Adding Years to Life* (2019).

94. Elshaer, M., Chen, Y., Wang, X. J. and Tang, X. Resveratrol: An overview of its anti-cancer mechanisms. *Life Sci* **207**, 340–349 (2018).

95. Ko, J. H., Sethi, G., Um, J. Y., Shanmugam, M. K., Arfuso, F., Kumar, A. P., Bishayee, A. and Ahn, K. S. The role of resveratrol in cancer therapy. *Int J Mol Sci* **18**, (2017).

96. Carrizzo, A., Izzo, C. and Vecchione, C. Protective Activity of Resveratrol in Cardio- and Cerebrovascular Diseases. *Resveratrol - Adding Life to Years, Not Adding Years to Life* (2019).

97. Bonnefont-Rousselot, D. Resveratrol and cardiovascular diseases. *Nutrients* **8**, (2016).

98. Tellone, E., Galtieri, A., Russo, A., Giardina, B. and Ficarra, S. Resveratrol: A focus on several neurodegenerative diseases. *Oxid Med Cell Longev* (2015).

99. Komorowska, J., Wątroba, M. and Szukiewicz, D. Review of beneficial effects of resveratrol in neurodegenerative diseases such as Alzheimer's disease. *Adv Med Sci* **65**, 415–423 (2020).

100. Varoni, E. M., lo Faro, A. F., Sharifi-Rad, J. and Iriti, M. Anticancer Molecular Mechanisms of Resveratrol. *Front Nutr* **3**, (2016).

101. Liu, Z., Li, Y. and Yang, R. Effects of resveratrol on vascular endothelial growth factor expression in osteosarcoma cells and cell proliferation. *Oncol Lett* **4**, 837–839 (2012).

102. Chen, G., Xia, H., Zhang, Z. guo and Yu, H. liang. Resveratrol in management of bone and spinal cancers. *Nat Prod Res* **33**, 516–526 (2019).

103. Lee, A. M. C., Shandala, T., Nguyen, L., Muhlhausler, B. S., Chen, K. M., Howe, P. R. and Xian, C. J. Effects of resveratrol supplementation on bone growth in young rats and microarchitecture and remodeling in ageing rats. *Nutrients* **6**, 5871–5887 (2014).

104. Martin, V. and Bettencourt, A. Bone regeneration: Biomaterials as local delivery systems with improved osteoinductive properties. *Materials Science and Engineering C* **82**, 363–371 (2018).

105. Wang, X., Chen, L. and Peng, W. Protective effects of resveratrol on osteoporosis via activation of the SIRT1-NF-κB signaling pathway in rats. *Exp Ther Med* **14**, 5032–5038 (2017).

106. Wong, R. H. X., Thaung Zaw, J. J., Xian, C. J. and Howe, P. R. C. Regular Supplementation With Resveratrol Improves Bone Mineral Density in Postmenopausal Women: A Randomized, Placebo-Controlled Trial. *Journal of Bone and Mineral Research* **35**, 2121–2131 (2020).

107. Zou, Y., Yang, J. and Jiang, D. Resveratrol inhibits canonical Wnt signaling in human MG-63 osteosarcoma cells. *Mol Med Rep* **12**, 7221–7226 (2015).

108. Peng, L. and Jiang, D. Resveratrol eliminates cancer stem cells of osteosarcoma by STAT3 pathway inhibition. *PLoS One* **13**, (2018).

109. Xu, N., Wang, L., Fu, S. and Jiang, B. Resveratrol is cytotoxic and acts synergistically with NF-κB inhibition in osteosarcoma MG-63 cells. *Archives of Medical Science* **17**, 166–176 (2021).

110. Mantyh, P. W. Bone cancer pain: From mechanism to therapy. *Curr Opin Support Palliat Care* **8**, 83–90 (2014).

111. Lux, S., Lobos, N., Lespay-Rebolledo, C., Salas-Huenuleo, E., Kogan, M. J., Flores, C., Pinto, M., Hernandez, A., Pelissier, T. and Constandil, L. The antinociceptive effect of resveratrol in bone cancer pain is inhibited by the Silent Information Regulator 1 inhibitor selisistat. *Journal of Pharmacy and Pharmacology* **71**, 816–825 (2019).

112. Zhu, H., Ding, J., Wu, J., Liu, T., Liang, J., Tang, Q. and Jiao, M. Resveratrol attenuates bone cancer pain through regulating the expression levels of ASIC3 and activating cell autophagy. *Acta Biochim Biophys Sin (Shanghai)* **49**, 1008–1014 (2017).

113. Belguendouz, L., Fremont, L. and Hard, A. Resveratrol Inhibits Metal Ion-Dependent and Independent Peroxidation of Porcine Low-Density Lipoproteins. *Biochem Pharmacol* **53**, 1347–1355 (1997).

114. Khan, M. A., Muzammil, S. and Musarrat, J. Differential binding of tetracyclines with serum albumin and induced structural alterations in drug-bound protein. *Int J Biol Macromol* **30**, 243–249 (2002).

115. López-Nicolás, J. M., Núñez-Delicado, E., Pérez-López, A. J., Barrachina, Á. C. and Cuadra-Crespo, P. Determination of stoichiometric coefficients and apparent formation constants for β-cyclodextrin complexes of trans-resveratrol using reversed-phase liquid chromatography. *J Chromatogr A* **1135**, 158–165 (2006).

116. Sergides, C., Chirilă, M., Silvestro, L., Pitta, D. and Pittas, A. Bioavailability and safety study of resveratrol 500 mg tablets in healthy male and female volunteers. *Exp Ther Med* **11**, 164–170 (2016).

117. Marier, J. F., Vachon, P., Gritsas, A., Zhang, J., Moreau, J. P. and Ducharme, M. P. Metabolism and disposition of resveratrol in rats: Extent of absorption, glucuronidation, and enterohepatic recirculation evidenced by a linked-rat model. *Journal of Pharmacology and Experimental Therapeutics* **302**, 369–373 (2002).

118. Walle, T., Hsieh, F., DeLegge, M. H., Oatis, J. E. and Walle, U. K. High absorption but very low bioavailability of oral resveratrol in humans. *Drug Metabolism and Disposition* **32**, 1377–1382 (2004).

119. Neves, A. R., Lúcio, M., Lima, J. L. C. and Reis, S. Resveratrol in Medicinal Chemistry: A Critical Review of its Pharmacokinetics, Drug-Delivery, and Membrane Interactions. *Curr Med Chem* **19**, 1663 (2012).

120. Machado, N. D., Fernández, M. A. and Díaz, D. D. Recent Strategies in Resveratrol Delivery Systems. *Chempluschem* **84**, 951–973 (2019).

121. Zupančič, Š., Lavrič, Z. and Kristl, J. Stability and solubility of trans-resveratrol are strongly influenced by pH and temperature. *European Journal of Pharmaceutics and Biopharmaceutics* **93**, 196–204 (2015).

122. Bhagwat, R. and Vaidhya, I. Novel Drug Delivery Systems: An Overview. *Int J Pharm Sci Res* **4**, 970–982 (2013).

123. Singh, G. and Pai, R. S. Recent advances of resveratrol in nanostructured based delivery systems and in the management of HIV/AIDS. *Journal of Controlled Release* **194**, 178–188 (2014).

124. Devi, P., Sharma, P., Rathore, C. and Negi, P. Novel Drug Delivery Systems of Resveratrol to Bioavailability and Therapeutic Effects. *Resveratrol - Adding Life to Years, Not Adding Years to Life* (2019).

125. Wang, C., He, C., Tong, Z., Liu, X., Ren, B. and Zeng, F. Combination of adsorption by porous CaCO3 microparticles and encapsulation by polyelectrolyte multilayer films for sustained drug delivery. *Int J Pharm* **308**, 160–167 (2006).

126. Singh, G. Resveratrol: Nanocarrier-based delivery systems to enhance its therapeutic potential. *Nanomedicine* **15**, 2801–2817 (2020).

127. Trollope, L., Cruickshank, D. L., Noonan, T., Bourne, S. A., Sorrenti, M., Catenacci, L. and Caira, M. R. Inclusion of trans-resveratrol in methylated cyclodextrins: Synthesis and solid-state structures. *Beilstein Journal of Organic Chemistry* **10**, 3136–3151 (2014).

128. Venuti, V., Cannavà, C., Cristiano, M. C., Fresta, M., Majolino, D., Paolino, D., Stancanelli, R., Tommasini, S. and Ventura, C. A. A characterization study of resveratrol/sulfobutyl ether-β-cyclodextrin inclusion complex and in vitro anticancer activity. *Colloids Surf B Biointerfaces* **115**, 22–28 (2014).

129. Soo, E., Thakur, S., Qu, Z., Jambhrunkar, S., Parekh, H. S. and Popat, A. Enhancing delivery and cytotoxicity of resveratrol through a dual nanoencapsulation approach. *J Colloid Interface Sci* **462**, 368–374 (2016).

130. Jhaveri, A., Deshpande, P., Pattni, B. and Torchilin, V. Transferrin-targeted, resveratrol-loaded liposomes for the treatment of glioblastoma. *Journal of Controlled Release* **277**, 89–101 (2018).

131. Huang, M., Liang, C., Tan, C., Huang, S., Ying, R., Wang, Y., Wang, Z. and Zhang, Y. Liposome co-encapsulation as a strategy for the delivery of curcumin and resveratrol. *Food Funct* **10**, 6447–6458 (2019).

132. Zu, Y., Overby, H., Ren, G., Fan, Z., Zhao, L. and Wang, S. Resveratrol liposomes and lipid nanocarriers: Comparison of characteristics and inducing browning of white adipocytes. *Colloids Surf B Biointerfaces* **164**, 414–423 (2018).

133. Lu, X., Ji, C., Xu, H., Li, X., Ding, H., Ye, M., Zhu, Z., Ding, D., Jiang, X., Ding, X. and Guo, X. Resveratrol-loaded polymeric micelles protect cells from Aβ-induced oxidative stress. *Int J Pharm* **375**, 89–96 (2009).

134. Peñalva, R., Morales, J., González-Navarro, C. J., Larrañeta, E., Quincoces, G., Peñuelas, I. and Irache, J. M. Increased oral bioavailability of resveratrol by its encapsulation in casein nanoparticles. *Int J Mol Sci* **19**, (2018).

135. Yang, C., Wang, Y., Xie, Y., Liu, G., Lu, Y., Wu, W. and Chen, L. Oat protein-shellac nanoparticles as a delivery vehicle for resveratrol to improve bioavailability in vitro and in vivo. *Nanomedicine* **14**, 2853–2871 (2019).

136. Santos, A. C., Pereira, I., Pereira-Silva, M., Ferreira, L., Caldas, M., Magalhães, M., Figueiras, A., Ribeiro, A. J. and Veiga, F. Nanocarriers for resveratrol delivery: Impact on stability and solubility concerns. *Trends Food Sci Technol* **91**, 483–497 (2019).

137. Narayan, R., Nayak, U. Y., Raichur, A. M. and Garg, S. Mesoporous silica nanoparticles: A comprehensive review on synthesis and recent advances. *Pharmaceutics* **10**, (2018).

138. Zhou, Y., Quan, G., Wu, Q., Zhang, X., Niu, B., Wu, B., Huang, Y., Pan, X. and Wu, C. Mesoporous silica nanoparticles for drug and gene delivery. *Acta Pharm Sin B* **8**, 165–177 (2018).

139. Desai, D., Åkerfelt, M., Prabhakar, N., Toriseva, M., Näreoja, T., Zhang, J., Nees, M. and Rosenholm, J. M. Factors affecting intracellular delivery and release of hydrophilic versus hydrophobic cargo from mesoporous silica nanoparticles on 2D and 3D cell cultures. *Pharmaceutics* **10**, (2018).

140. Slowing, I. I., Vivero-Escoto, J. L., Wu, C. W. and Lin, V. S. Y. Mesoporous silica nanoparticles as controlled release drug delivery and gene transfection carriers. *Adv Drug Deliv Rev* **60**, 1278–1288 (2008).

141. Qin, L., He, Y., Zhao, X., Zhang, T., Qin, Y. and Du, A. Preparation, Characterization, and in Vitro Sustained Release Profile of Resveratrol-Loaded Silica Aerogel. *Molecules* **25**, (2020).

142. Wang, Y., Kao, Z., Zhang, T., Zhang, Y., Qin, L., Zhang, Z., Zhou, B., Wu, G., Shen, J. and Du, A. Diffusion of resveratrol in silica alcogels. *Molecules* **24**, (2019).

143. Marinheiro, D., Ferreira, B. J. M. L., Oskoei, P., Oliveira, H. and Daniel-da-silva, A. L. Encapsulation and enhanced release of resveratrol from mesoporous silica nanoparticles for melanoma therapy. *Materials* **14**, 1–18 (2021).

144. Chaudhary, Z., Subramaniam, S., Khan, G. M., Abeer, M. M., Qu, Z., Janjua, T., Kumeria, T., Batra, J. and Popat, A. Encapsulation and Controlled Release of Resveratrol Within Functionalized Mesoporous Silica Nanoparticles for Prostate Cancer Therapy. *Front Bioeng Biotechnol* **7**, (2019).

145. Juère, E., Florek, J., Bouchoucha, M., Jambhrunkar, S., Wong, K. Y., Popat, A. and Kleitz, F. In Vitro Dissolution, Cellular Membrane Permeability, and Anti-Inflammatory Response of Resveratrol-Encapsulated Mesoporous Silica Nanoparticles. *Mol Pharm* **14**, 4431–4441 (2017).

146. Hu, Y., Wang, Z., Qiu, Y., Liu, Y., Ding, M. and Zhang, Y. Anti-miRNA21 and resveratrol-loaded polysaccharide-based mesoporous silica nanoparticle for synergistic activity in gastric carcinoma. *J Drug Target* **27**, 1135–1143 (2019).

147. Juère, E., Florek, J., Bouchoucha, M., Jambhrunkar, S., Wong, K. Y., Popat, A. and Kleitz, F. In Vitro Dissolution, Cellular Membrane Permeability, and Anti-Inflammatory Response of Resveratrol-Encapsulated Mesoporous Silica Nanoparticles. *Mol Pharm* **14**, 4431–4441 (2017).

148. Summerlin, N., Qu, Z., Pujara, N., Sheng, Y., Jambhrunkar, S., McGuckin, M. and Popat, A. Colloidal mesoporous silica nanoparticles enhance the biological activity of resveratrol. *Colloids Surf B Biointerfaces* **144**, 1–7 (2016).

149. Bernard Dennis Cullity. *Elements of x-ray diffraction*. (Addison-Wesley Publishing Company Inc., 1978).

150. Bunaciu, A. A., Udriştioiu, E. gabriela and Aboul-Enein, H. Y. X-Ray Diffraction: Instrumentation and Applications. *Crit Rev Anal Chem* **45**, 289–299 (2015).

151. Holder, C. F. and Schaak, R. E. Tutorial on Powder X-ray Diffraction for Characterizing Nanoscale Materials. *ACS Nano* **13**, 7359–7365 (2019).

152. Kim, S. H., Lee, C. M. and Kafle, K. Characterization of crystalline cellulose in biomass: Basic principles, applications, and limitations of XRD, NMR, IR, Raman, and SFG. *Korean Journal of Chemical Engineering* **30**, 2127–2141 (2013).

153. Dutta, A. Fourier Transform Infrared Spectroscopy. *Spectroscopic Methods for Nanomaterials Characterization* **2**, 73–93 (2017).

154. Bacsik, Z., Mink, J. and Keresztury, G. FTIR spectroscopy of the atmosphere. I. Principles and methods. *Appl Spectrosc Rev* **39**, 295–363 (2004).

155. Capeletti, L. B. and Zimnoch, J. H. Fourier Transform Infrared and Raman Characterization of Silica-Based Materials. *Applications of Molecular Spectroscopy to Current Research in the Chemical and Biological Sciences* (2016).

156. Melucci, D., Zappi, A., Poggioli, F., Morozzi, P., Giglio, F. and Tositti, L. ATR-FTIR spectroscopy, a new non-destructive approach for the quantitative determination of biogenic silica in marine sediments. *Molecules* **24**, (2019).

157. Efstathiou, A. M., Gleavs, J. T. and Yablonsky, G. S. Characterization of Solid Materials and Heterogeneous Catalysts - Transient Techniques: Temporal Analysis of Products and Steady State Isotopic Transient Kinetics Analysis. *Characterization of Solid Materials and Heterogeneous Catalysts, Volume 2 of 2* 1013–1073 (2012).

158. Ambroz, F., Macdonald, T. J., Martis, V. and Parkin, I. P. Evaluation of the BET theory for the characterization of meso and microporous MOFs. *Small Methods* **2**, (2018).

159. Sing, K. S. W., Everett, D. H., Haul, R. A. W., Moscou, L., Pierotti, R. A., Rouquerol, J. and Siemieniewska, T. Reporting Physisorption Data for Gas/Solid Systems with Special Reference to the Determination of Surface Area and Porosity. *Pure and Applied Chemistry* **57**, 603–619 (1985).

160. Sing, K. S. W., Everett, D. H., Haul, R. A. W., Moscou, L., Pierotti, R. A., Rouquerol, J. and Siemieniewska, T. Reporting Physisorption Data for Gas/Solid Systems with Special Reference to the Determination of Surface Area and Porosity. *Pure and Applied Chemistry* **57**, 603–619 (1985).

161. Catauro, M. and Ciprioti, S. V. Characterization of hybrid materials prepared by sol-gel method for biomedical implementations. A critical review. *Materials* **14**, (2021).

162. Abd Mutalib, M., Rahman, M. A., Othman, M. H. D., Ismail, A. F. and Jaafar, J. Scanning Electron Microscopy (SEM) and Energy-Dispersive X-Ray (EDX) Spectroscopy. *Membrane Characterization* 161–179 (2017).

163. Vernon-Parry, K. D. Scanning Electron Microscopy: an introduction. *III- Vs Review* **13**, 40–44 (2000).

164. Coats, A. W. and Redfern, J. P. Thermogravimetric analysis. A review. *Analyst* **88**, 906–924 (1963).

165. Twentyman, P. R. and Luscombe, M. A study of some variables in a tetrazolium dye (MTT) based assay for cell growth and chemosensitivity. *Br. J. Cancer* **56**, 279–285 (1987).

166. van Meerloo, J., Kaspers, G. J. L. and Cloos, J. Cell Sensitivity Assays: The MTT Assay. *Methods in Molecular Biology* **731**, 237–245 (2011).

167. Brus, J. and Dybal, J. Solid-state NMR study of structure, size and dynamics of domains in hybrid siloxane networks. *Polymer (Guildf)* **41**, 5269–5282 (2000).

168. Yoshino, H., Kamiya, K. and Nasu, H. IR study on the structural evolution of sol-gel derived SiO 2 gels in the early stage of conversion to glasses. *J Non Cryst Solids* **126**, 68–78 (1990).

169. Almeida, J. C., Wacha, A., Bóta, A., Almásy, L., Vaz Fernandes, M. H., Margaça, F. M. A. and Miranda Salvado, I. M. PDMS-SiO2 hybrid materials - A new insight into the role of Ti and Zr as additives. *Polymer (Guildf)* **72**, 40–51 (2015).

170. Almeida, J. C., Castro, A. G. B., Lancastre, J. J. H., Miranda Salvado, I. M., Margaça, F. M. A., Fernandes, M. H. V., Ferreira, L. M. and Casimiro, M. H. Structural characterization of PDMS-TEOS-CaO-TiO2 hybrid materials obtained by sol-gel. *Mater Chem Phys* **143**, 557–563 (2014).

171. Pêna, R., Pêna-Alonso, P., Rubio, J., Rubio, F. and Oteo, J. L. A FT-IR Study of the Synthesis of Boron Ormosils by Means of the Sol-Gel Process. *J Solgel Sci Technol* **25**, 255–263 (2002).

172. Rubio, F., Rubio, J. and Oteo, J. L. A FT-IR study of the hydrolysis of Tetraethylorthoselicate (TEOS). *Spectroscopy Letters* **31**, 199–219 (1998).

173. Manzano, M., Salinas, A. J., Gil, F. J. and Vallet-Regí, M. Mechanical properties of organically modified silicates for bone regeneration. *J Mater Sci Mater Med* **20**, 1795–1801 (2009).

174. Zhang, X. X., Xia, B. B., Ye, H. P., Zhang, Y. L., Xiao, B., Yan, L. H., Lv, H. B. and Jiang, B. One-step sol–gel preparation of PDMS–silica ORMOSILs as environment-resistant and crack-free thick antireflective coatings. *J Mater Chem* **22**, 13132–13140 (2012).

175. Almeida, J. C., Lancastre, J., Vaz Fernandes, M. H., Margaça, F. M. A., Ferreira, L. and Miranda Salvado, I. M. Evaluating structural and microstructural changes of

PDMS -SiO2 hybrid materials after sterilization by gamma irradiation. *Materials Science and Engineering C* **48**, 354–358 (2015).

176. Aguiar, H., Serra, J., González, P. and León, B. Structural study of sol-gel silicate glasses by IR and Raman spectroscopies. *J Non Cryst Solids* **355**, 475–480 (2009).

177. Illescas, J. F. and Mosquera, M. J. Surfactant-synthesized PDMS/silica nanomaterials improve robustness and stain resistance of carbonate stone. *Journal of Physical Chemistry C* **115**, 14624–14634 (2011).

178. Fehr, S. M. and Krossing, I. Spectroscopic Signatures of Pressurized Carbon Dioxide in Diffuse Reflectance Infrared Spectroscopy of Heterogeneous Catalysts. *ChemCatChem* **12**, 2622–2629 (2020).

179. Catenacci, L., Sorrenti, M., Bonferoni, M. C., Hunt, L. and Caira, M. R. Inclusion of the phytoalexin trans-resveratrol in native cyclodextrins: A thermal, spectroscopic, and X-ray structural study. *Molecules* **25**, (2020).

180. Trollope, L., Cruickshank, D. L., Noonan, T., Bourne, S. A., Sorrenti, M., Catenacci, L. and Caira, M. R. Inclusion of trans-resveratrol in methylated cyclodextrins: Synthesis and solid-state structures. *Beilstein Journal of Organic Chemistry* **10**, 3136–3151 (2014).

181. Ansari, K. A., Vavia, P. R., Trotta, F. and Cavalli, R. Cyclodextrin-based nanosponges for delivery of resveratrol: In vitro characterisation, stability, cytotoxicity and permeation study. *AAPS PharmSciTech* **12**, 279–286 (2011).

182. Gumireddy, A., Christman, R., Kumari, D., Tiwari, A., North, E. J. and Chauhan, H. Preparation, Characterization, and In vitro Evaluation of Curcumin- and Resveratrol-Loaded Solid Lipid Nanoparticles. *AAPS PharmSciTech* **20**, (2019).

183. Silva, R. de C. da, Teixeira, J. A., Nunes, W. D. G., Zangaro, G. A. C., Pivatto, M., Caires, F. J. and Ionashiro, M. Resveratrol: A thermoanalytical study. *Food Chem* **237**, 561–565 (2017).

184. Zupančič, Š., Lavrič, Z. and Kristl, J. Stability and solubility of trans-resveratrol are strongly influenced by pH and temperature. *European Journal of Pharmaceutics and Biopharmaceutics* **93**, 196–204 (2015).

185. Fritz, B., Lach, J. L. and Bighley, L. D. Solubility Analysis of Multicomponent Systems Capable of Interacting in Solution. *American Can Co* **60**, (1971).

186. Peppas, N. A. and Narasimhan, B. Mathematical models in drug delivery: How modeling has shaped the way we design new drug delivery systems. *Journal of Controlled Release* **190**, 75–81 (2014).

187. Costa, P., Manuel, J. and Lobo, S. Modeling and comparison of dissolution profiles. *European Journal of Pharmaceutical Sciences* **13**, 123–133 (2001).

188. Ritger, P. L. and Peppas, N. A. A simple equation for description of solute release I. Fickian and non-fickian release from non-swellable devices in the form of slabs, spheres, cylinders or discs. *Journal of Controlled Release* **5**, 23–36 (1987).

189. Korsmeyer, R. W., Gurny, R., Doelker, E., Buri, P. and Peppas, N. A. Mechanisms of solute release from porous hydrophilic polymers. *Int J Pharm* **15**, 25–35 (1983).

190. Waloddi Weibull. A Statistical Distribution Function of Wide Applicability. *J Appl Mech* 293–297 (1951).

191. Langenbucher, F. Letters to the Editor: Linearization of dissolution rate curves by the Weibull distribution. *Journal of Pharmacy and Pharmacology* **24**, 979–981 (1972).

192. Prezotti, F. G., Boni, F. I., Ferreira, N. N., de Souza e Silva, D., Campana-Filho, S. P., Almeida, A., Vasconcelos, T., Gremião, M. P. D., Cury, B. S. F. and Sarmento, B. Gellan gum/pectin beads are safe and efficient for the targeted colonic delivery of resveratrol. *Polymers (Basel)* **10**, (2018).

193. Ji, S., Jia, C., Cao, D., Muhoza, B. and Zhang, X. Formation, characterization and properties of resveratrol-dietary fiber composites: Release behavior, bioaccessibility and long-term storage stability. *LWT* **129**, (2020).

194. Cardoso, T., Gonçalves, A., Estevinho, B. N. and Rocha, F. Potential food application of resveratrol microparticles: Characterization and controlled release studies. *Powder Technol* **355**, 593–601 (2019).

195. Chellappa, M., Thejaswini, B. and Vijayalakshmi, U. Biocompatibility assessment of SiO2-TiO2 composite powder on MG63 osteoblast cell lines for orthopaedic applications. in *IET Nanobiotechnology* vol. 11 77–82 (Institution of Engineering and Technology, 2017).

196. Tavakoli, S., Nemati, S., Kharaziha, M. and Akbari-Alavijeh, S. Embedding CuO Nanoparticles in PDMS-SiO2 Coating to Improve Antibacterial Characteristic and Corrosion Resistance. *Colloids and Interface Science Communications* **28**, 20–28 (2019).

197. Meng Bao, C. le, Y.L., E., S.K., M., Liu, Y., Choolani, M. and K.Y., J. Advances in Bone Tissue Engineering. *Regenerative Medicine and Tissue Engineering* (2013).

198. Almeida, J. C., Wacha, A., Bóta, A., Almásy, L., Vaz Fernandes, M. H., Margaça, F. M. A. and Miranda Salvado, I. M. PDMS-SiO2 hybrid materials - A new insight into the role of Ti and Zr as additives. *Polymer (Guildf)* **72**, 40–51 (2015).

Supplementary material

Calibration curves for RES

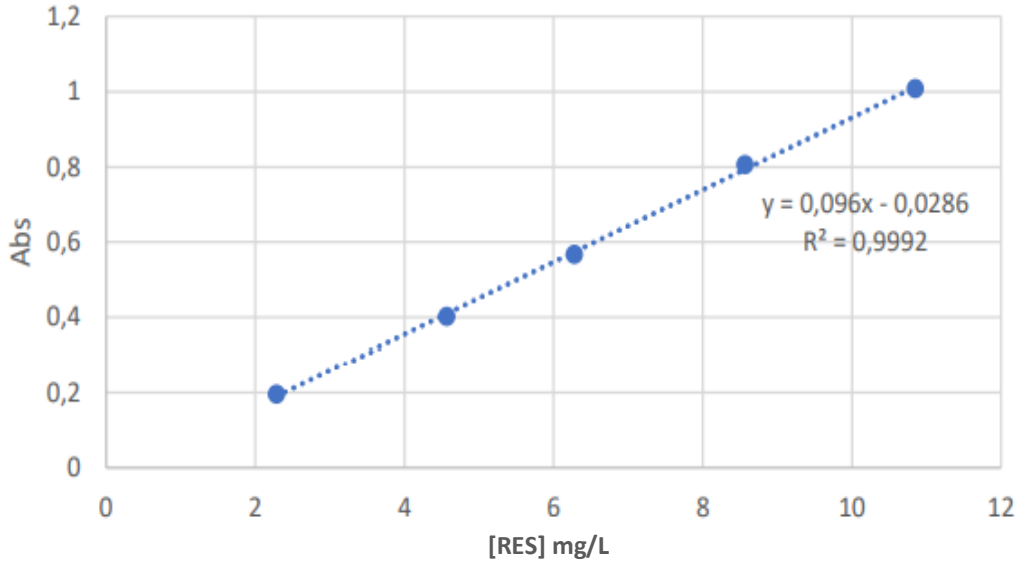

Figure sm1. Calibration curve for RES at PBS pH 5.2.

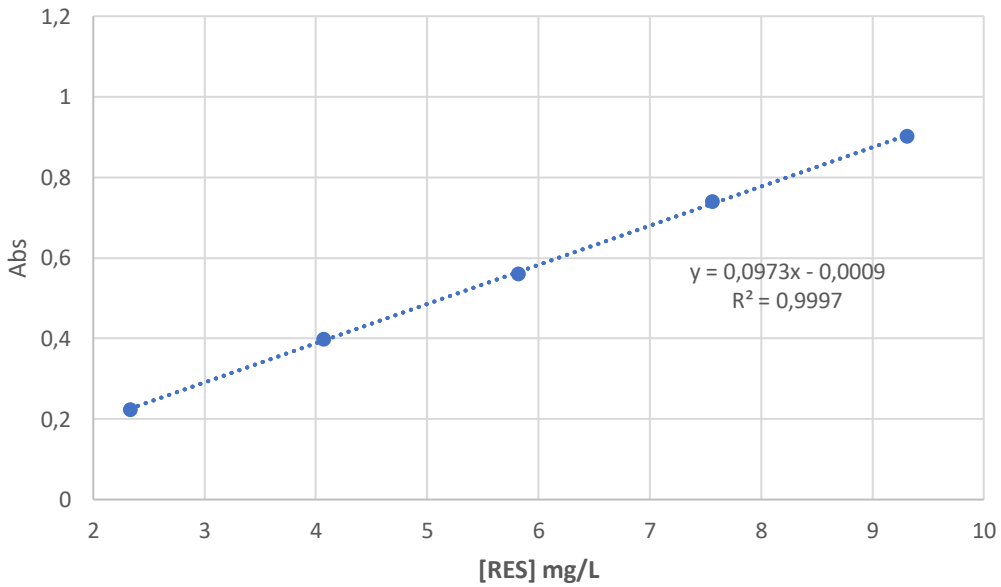

Figure sm2. Calibration curve for RES at PBS pH 7.4.

RES release studies spectra

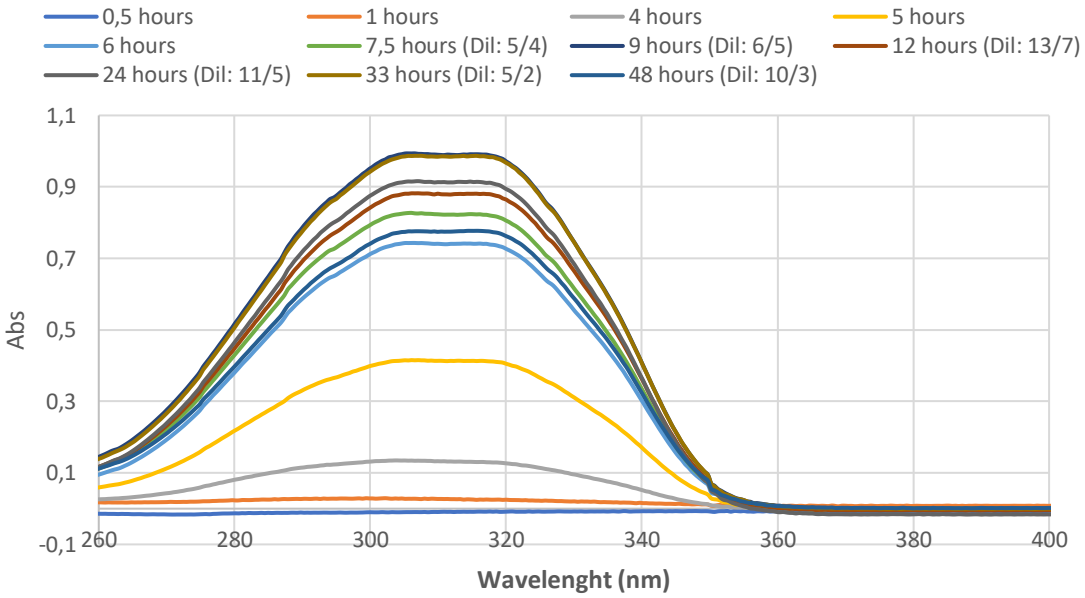

Figure sm3. RES spectra obtained at various times for the sample M0CO-IV-RES at pH 5.2 (with the respective dilutions used).

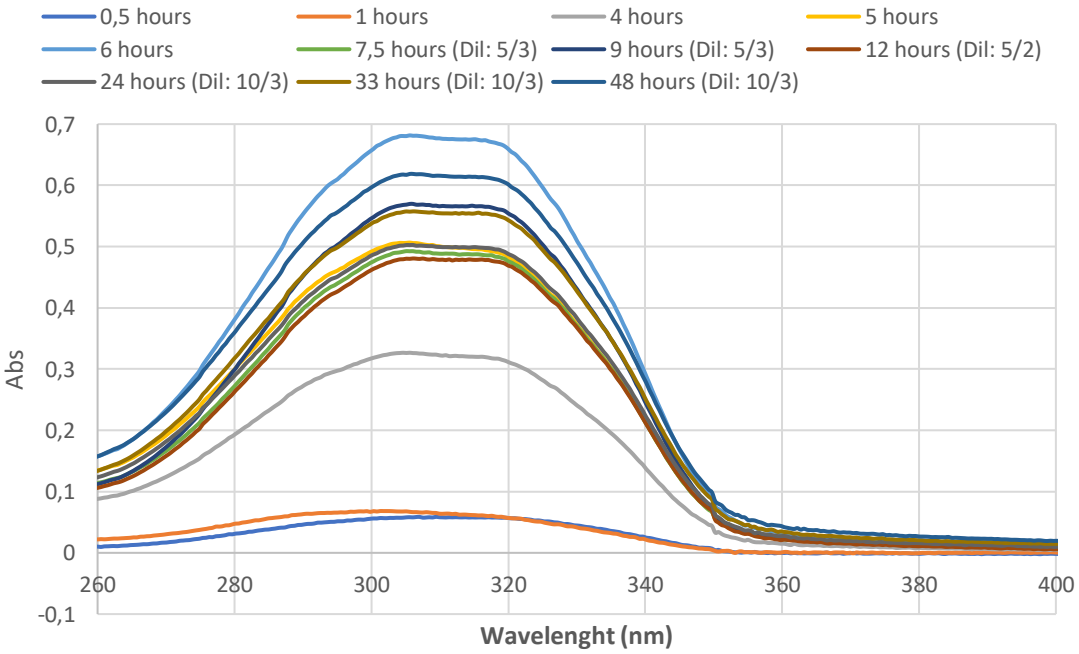

Figure sm4. RES spectra obtained at various times for the sample M0CO-IV-RES at pH 7.4 (with the respective dilutions used).